Chapter 3

Results and Discussion

Section (1)

Cyclic voltammograms of tin electrode in $NaHCO_3$ and NaCl solutions

The cyclic voltammograms technique is useful for identifying the electrochemical steps involved in the overall electrochemical reaction resulting in the formation of various films on the metallic surface [95-97]. The cyclic voltammetry is perhaps the most effective and versatile electroanalytical technique available for mechanistic study of the redox systems [98-99]. It enables the electrode potential to be readily scanned in search of redox-couples. Once located, a couple can then be characterized from the potentials of peaks on the cyclic voltammogram and from changes caused by the variation of the scanning rate [100].

3.1.1 Cyclic voltammograms of tin electrode in $NaHCO_3$ solutions.

Fig. (3.1) represents the anodic cyclic voltammogram curves of tin electrode in various concentrations of $NaHCO_3$ solutions. The curves were swept between -3000 mV and 3000 mV (SCE) at scan rate 1000 mV/sec. The data reveals that the anodic cyclic voltammogram contains two dissolution peaks (peak AI and shoulder peak AII), permanent passive and transpassive peak (peak AIII) regions. Peak AI can be assigned to the electroformation of $Sn(OH)_2$ and/or SnO according to the following reactions:

$$Sn + 2H_2O \rightarrow Sn(OH)_2 + 2H^+ + 2e^- \quad (3.1)$$

$$Sn(OH)_2 \rightarrow SnO + H_2O \quad (3.2)$$

Shah et al. [101] suggested that the stannous oxide does not form directly from tin but the initial product of the reaction is stannous hydroxide according to the following reaction:

$$Sn + 2OH^- \rightarrow Sn(OH)_2 + 2e^- \quad (3.3)$$

Two further reactions, one involving dehydration of stannous hydroxide, according to equation (3.2), and the other involving dissolution of tin as stannite ion, may take place:

$$Sn + 3OH^- \rightarrow HSnO_2^- + H_2O + 2e^- \quad (3.4)$$

Results by Garraett and Heiks [102] and by Kerr and MacNaughten [103] also indicate that tin dissolves in alkaline solution as stannite [$HSnO_2^-$] ions. The potential range of peak AII may be correlated with the formation of $Sn(OH)_4$ and/or SnO_2 according to the following equations [104]:

$$Sn(OH)_2 + 2OH^- \rightarrow Sn(OH)_4 + 2e^- \quad (3.5)$$

and

$$SnO + 2OH^- + H_2O \rightarrow Sn(OH)_4 + 2e^- \quad (3.6)$$

It may, therefore, be concluded that the more general reactions that occur within the peak AII region are the electrooxidation of $Sn(OH)_2$ and SnO to $Sn(OH)_4$ then dehydration of stannic hydroxide to stannic oxide.

$$Sn(OH)_4 \rightarrow SnO_2 + 2H_2O \quad (3.7)$$

Both SnO and SnO_2, dissolve in the alkaline media to yield stannite and stannate, respectively [105], so the stannic oxide may be present as stannate ion:

$$Sn + 5OH^- \rightarrow HSnO_3^- + 2H_2O + 4e^- \quad (3.8)$$

The height of peak AI is greater than that of peak AII in all cases. Beyond peak AII the dissolution current drops to small value, I_{pass}, indicating the onset of passivation. In passive region I_{pass} decreases slowly as the potential are moved in positive direction and this decreases may be explained on the basis that tin hydroxide is thermodynamically unstable with respect to the corresponding oxide and it is clear that the dehydration of hydroxides can occur on the electrode surface during the potential sweep to positive direction, hence the passive film becomes the more compact and, therefore, protective [106]. Previous works confirmed duplex nature of the passive film, which consists of both SnO and SnO_2 [107]. The region beyond the passivity plateau (peak AIII) cannot be assigned to any particular anodic oxidation reaction. Several authors [108] attributed the observation of the transpassive region in alkaline media to a solid phase transformation. It is generally believed that oxygen evolution occurs most probably on a film of metastannic acid (H_2SnO_3) [109]. The data of Fig. (1) reveals that the increase of the $NaHCO_3$ content causes an increase in the current density values of peaks AI, AII and AIII, at the same time these peaks shifted towards more negative potential values. The relation between the peak current density of peak AI vs. log [$NaHCO_3$] is given in Fig. (3.2). Reasonable linear dependence is shown, indicating as the concentration of $NaHCO_3$ increases the current density of peak AI increases.

Fig. (3.3) shows the cyclic voltammogram curves of tin electrode in 0.1M $NaHCO_3$ solution at scan rate 1000 mV/sec at various anodic potential limits. If the anodic sweep has been reversed at potential more positive than peak AIII, three reduction peaks (CI, CII and CIII) were appeared. If the anodic sweep has been reversed at potential values between peak AII and peak AIII, two reduction peaks (CI and CII) were appeared. If the anodic sweep has been reversed at potential values between peak AI and peak AII, only one reduction peak (peak CI) was appeared. This results show that peak CI results from the reduction of SnO and/or $Sn(OH)_2$, while peak CII results from the reduction of SnO_2 and/or $Sn(OH)_4$.

Fig. (3.4) represents the cyclic voltammogram curves of tin electrode in 0.1 M $NaHCO_3$ solution at different scan rates. Inspection of this figure it is clear that the peak current density for all peaks increases with increasing the scan rate.

Fig. (3.5) shows the relation between anodic peak current I_{PAI} versus the square root of scan rate, $\upsilon^{1/2}$, in 0.1 M $NaHCO_3$ solution. Good linearity was observed through the origin, this indicates that the participation of diffusion process in anodic reactions [110].

For diffusion controlled process under potentiodynamic condition, the slope of I_{PAI} versus $\upsilon^{1/2}$ relation are proportional to the concentration of diffusing species and to the square root of their diffusion coefficient according to Randles Sevik equation [111]:

$$I_{PA} = abZ^{1/2} CD^{1/2} \upsilon^{1/2} \qquad (3.9)$$

where a and b are constants, Z is the number of exchanged electrons, C is the concentration, D is the diffusion coefficient of the diffusing species and υ is the scan rate.

Fig. (3.6) shows the cyclic voltammograms for tin electrode in 0.1 M $NaHCO_3$ at scan rate 1000 mV/s under the influence of the successive cycling. The data shows that the current passing through the whole range decreases with the number of cycle. The difference in the form of the first and the subsequent cycles was explained by Gottesfeld [112] by the assumption that, at the completion of the first cycle a small fraction of the passive film remains unreduced. This is a result of some sluggishness in the process of decharging, caused by the increase in the resistance of the film against the completion of the reduction. The second cycle thus begins with a passive film that has not been reduced completely back to its initial condition.

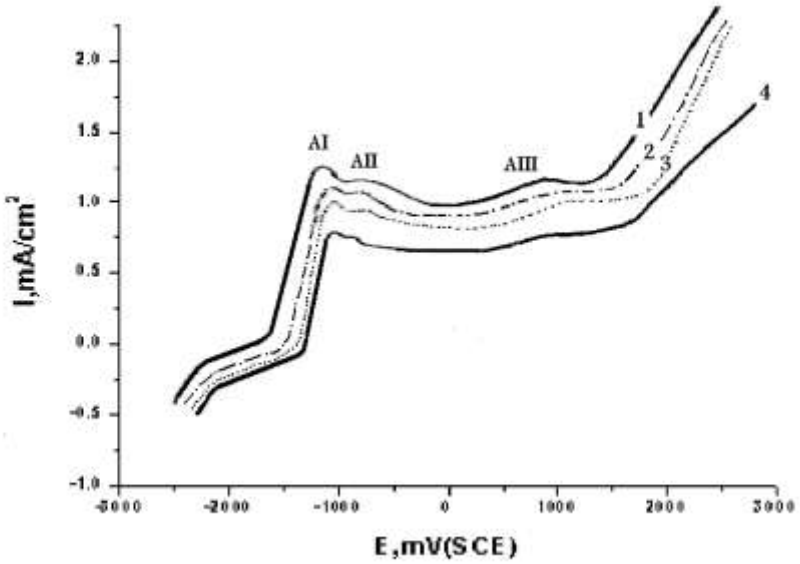

Fig.(3.1): Anodic cyclic voltammograms for tin electrode at various concentrations of $NaHCO_3$ and scan rate 1000 mV/sec. (1) 0.2, (2) 0.1, (3) 0.05 and (4) 0.01 M.

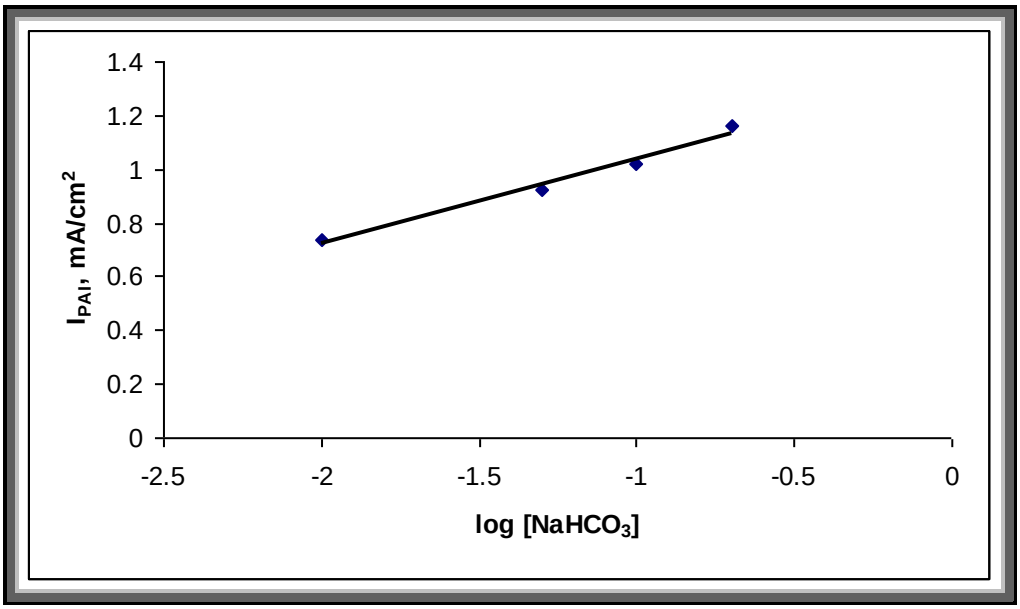

Fig.(3.2): The relation between (I_{PAI}) versus log [$NaHCO_3$] for tin electrode at scan rate 1000 mV/sec.

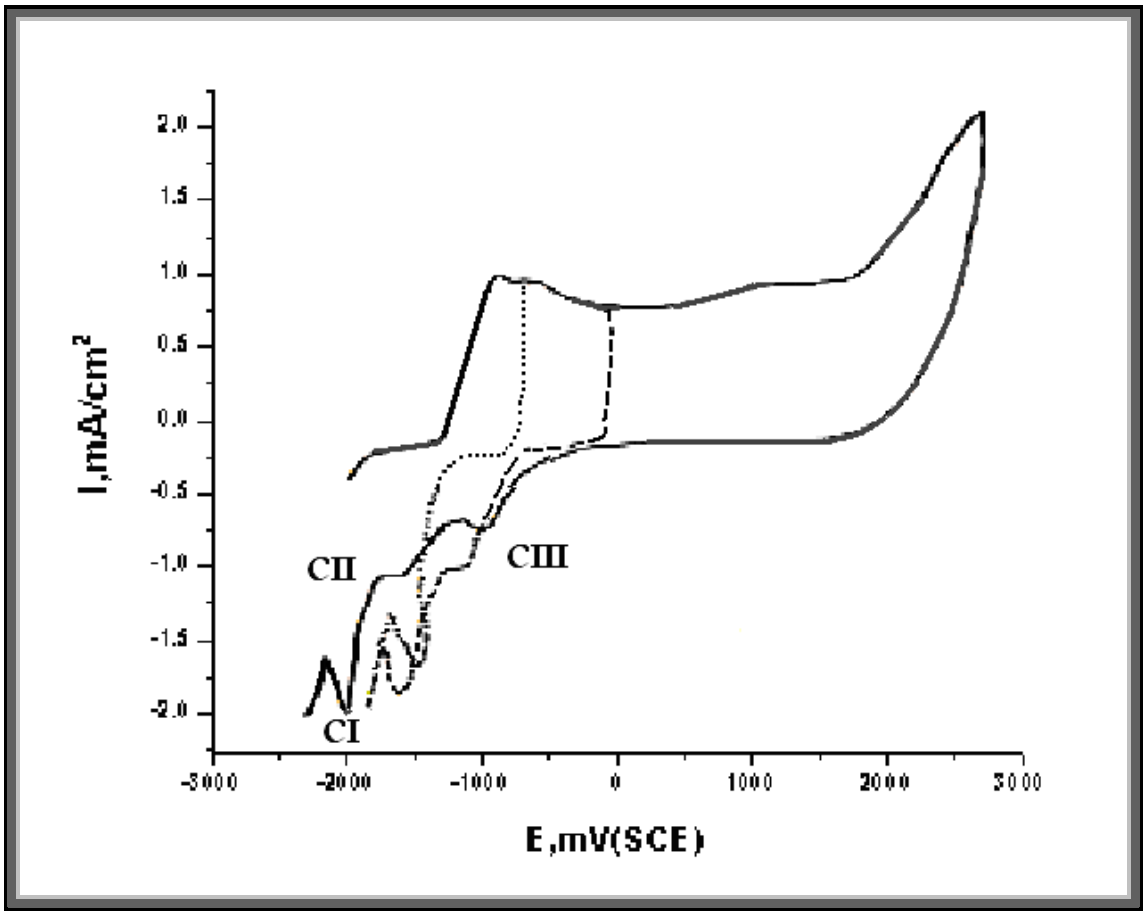

Fig.(3.3): Cyclic voltammograms for tin electrode in 0.1 M $NaHCO_3$ solution at scan rate 1000 mV/sec, starting at -3000 mV and reversed at various anodic potential limits.

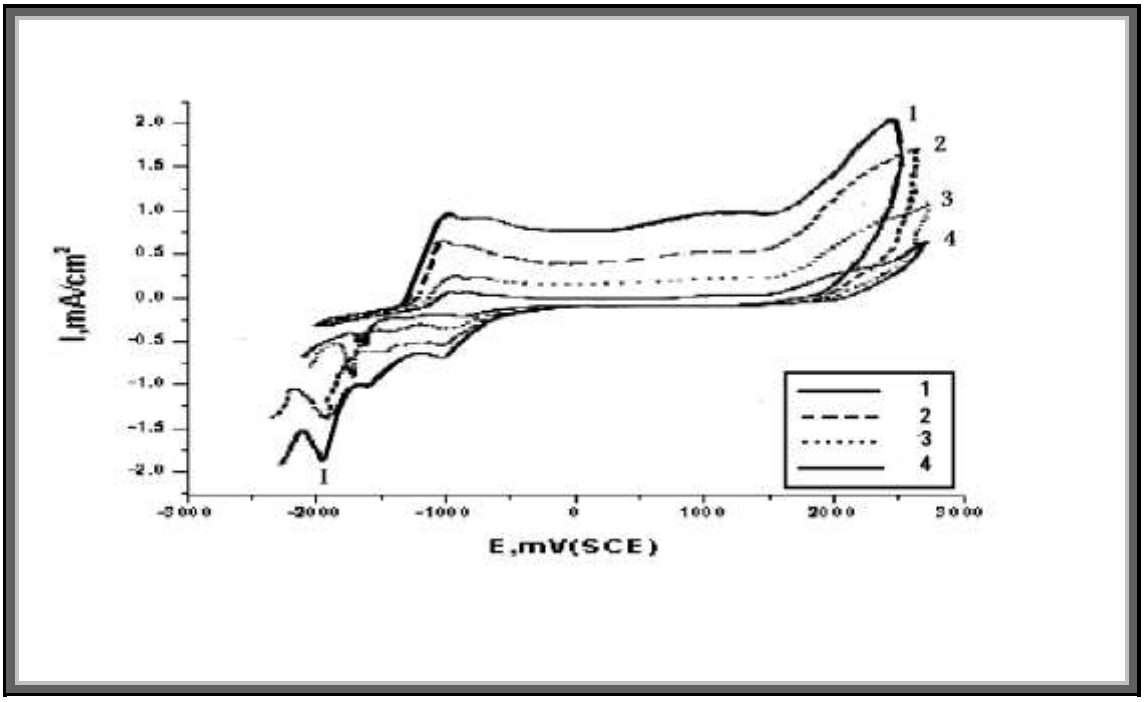

Fig.(3.4): Cyclic voltammograms for tin electrode in 0.1 M $NaHCO_3$ solution at different scan rates (1) 1000, (2) 500, (3) 250 and (4) 100 mV/sec.

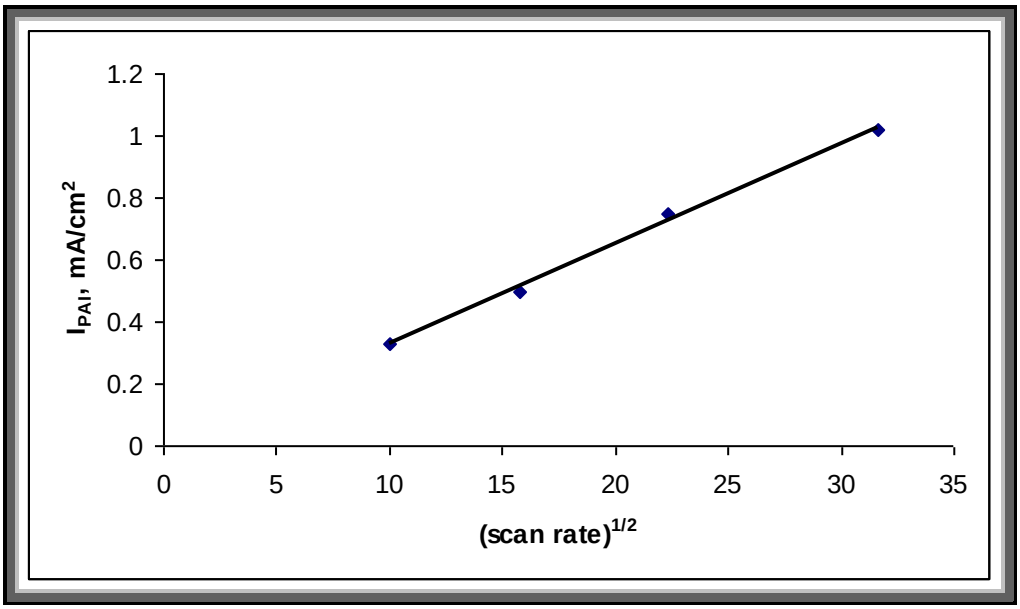

Fig.(3.5): Relation between (I_{PAI}) versus (scan rate)$^{1/2}$ for tin electrode in 0.1 M $NaHCO_3$ solution.

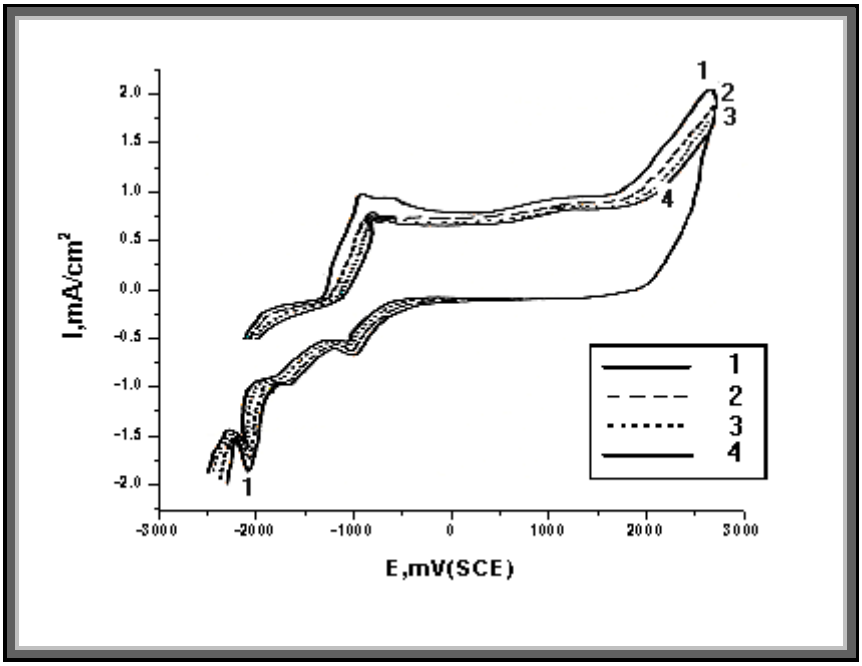

Fig.(3.6): Successive cyclic voltammograms for tin electrode in 0.1 M $NaHCO_3$ solution at scan rate 1000 mV/sec.

3.1.2 Cyclic voltammograms of tin electrode in NaCl solutions.

Fig. (3.7) represents the anodic cyclic voltammogram curves of tin electrode in various concentrations of NaCl solutions. The curves were swept between -2000 mV and 0 mV (SCE) at scan rate 100 mV/sec. The positive-going potential scan exhibit two anodic peaks (AI and AII). Peak AI can be assigned to the electroformation of $Sn(OH)_2$ and/or SnO according to data in the literature [76,88,101,113], the initial stages of tin passivity are the formation of $Sn(OH)_2$ according to equation (3.3), which dehydrates to form more stable SnO according to equation (3.2).

The potential range of peak AII may be correlated with the formation of $Sn(OH)_4$ and/or SnO_2 according to the equations (3.5-3.7).

Another electrode reaction may be involved in the case of chloride solution. According to Hoar [114], the development of a dense white film (tin-oxy chloride) occurs by the reaction:

$$Sn^{2+} + Cl^- + 2H_2O_{\text{liquid}} \rightarrow Sn(OH)ClH_2O_{\text{solid}} + H^+ \qquad (3.10)$$

When the surface is covered with the passive film, the dissolution current falls to a small value (I_{pass}) indicating the onset of permanent passivation. Previous works confirmed duplex nature of the passive film, which consists of both SnO and SnO_2 [107]. It is observed that at a certain critical potential (pitting potential E_{pit}), the passive current density increases steeply without any sign for oxygen evolution. The rapid rise in anodic current density at E_{pit} indicates initiation and growth of pitting attack. In this case, the aggressiveness of halide ions on the transpassive dissolution of tin in chloride solution could be attributed to formation of the soluble complex species [115]. Breakdown of the permanent passive layer and initiation of pitting attack can be ascribed as a competitive adsorption

between Cl^- ions and oxygenated species at adsorption sites on oxide covered layer [116]. Moreover, the adsorbed Cl^- ions can penetrate through the passive layer especially at its point defects and flow with the assistance of high electric field across the passive film to reach the base metal surface and initiate pitting [117]. The data of Fig. (3.7) reveals that the increase of the NaCl content causes an increase in the current density values of peaks AI and AII, at the same time these peaks shifted towards more negative potential values. The relation between the peak current density of peak AI vs. log [NaCl] is given in Fig. (3.8). Reasonable linear dependence is shown, indicating as the concentration of NaCl increases the current density of peak AI increases.

Fig. (3.9) shows the cyclic voltammogram curves of tin electrode in 0.6 M NaCl at scan rate 100 mV/sec at various anodic potential limits. During the potential sweep reversal, hystersis loop characteristic of localized corrosion phenomenon is observed. The cathodic excursion exhibits two cathodic peaks (CI and CII). If the anodic sweep has been reversed at potential more negative than E_{pit}, only one cathodic peak (peak CI) was appeared. So the cathodic peak CII can be assigned to the reduction of pitting corrosion products and the cathodic peak CI can be assigned to the reduction of the passive layer.

Fig. (3.10) shows the cyclic voltammogram curves of tin electrode in 0.6 M NaCl at scan rate 100 mV/sec under the influence of the successive cycling. The data shows that the current passing through the whole range decreases with the number of cycle. The difference in the form of the first and the subsequent cycles was explained by Gottesfeld [112] by the assumption that, at the completion of the first cycle a small fraction of the passive film remains unreduced. This is a result of some sluggishness in the process of decharging, caused by the increase in the resistance of the

film against the completion of the reduction. The second cycle thus begins with a passive film that has not been reduced completely back to its initial condition.

Fig. (3.11) represents the anodic cyclic voltammogram curves of tin electrode in 0.6 M NaCl solution. The curves were swept between -2000 mV and 0 mV (SCE) at different scan rates. From Fig. (3.11), it is observed that the increasing of the scan rate increases the current density of the two anodic peaks and E_{pit} shifted towards more positive potentials. Such behavior is explained in terms of incubation time [110]. When υ is high, pitting initiation occurs only at more positive potentials, corresponding to sufficient short incubation time, i.e, time needed to perforate the passive layer.

Fig. (3.12) shows the linear relation between anodic peak current density I_{PAI} and $\upsilon^{1/2}$ in 0.6 M NaCl solution. Good linearity was observed near the origin, this indicates that the participation of diffusion process in anodic reactions [110].

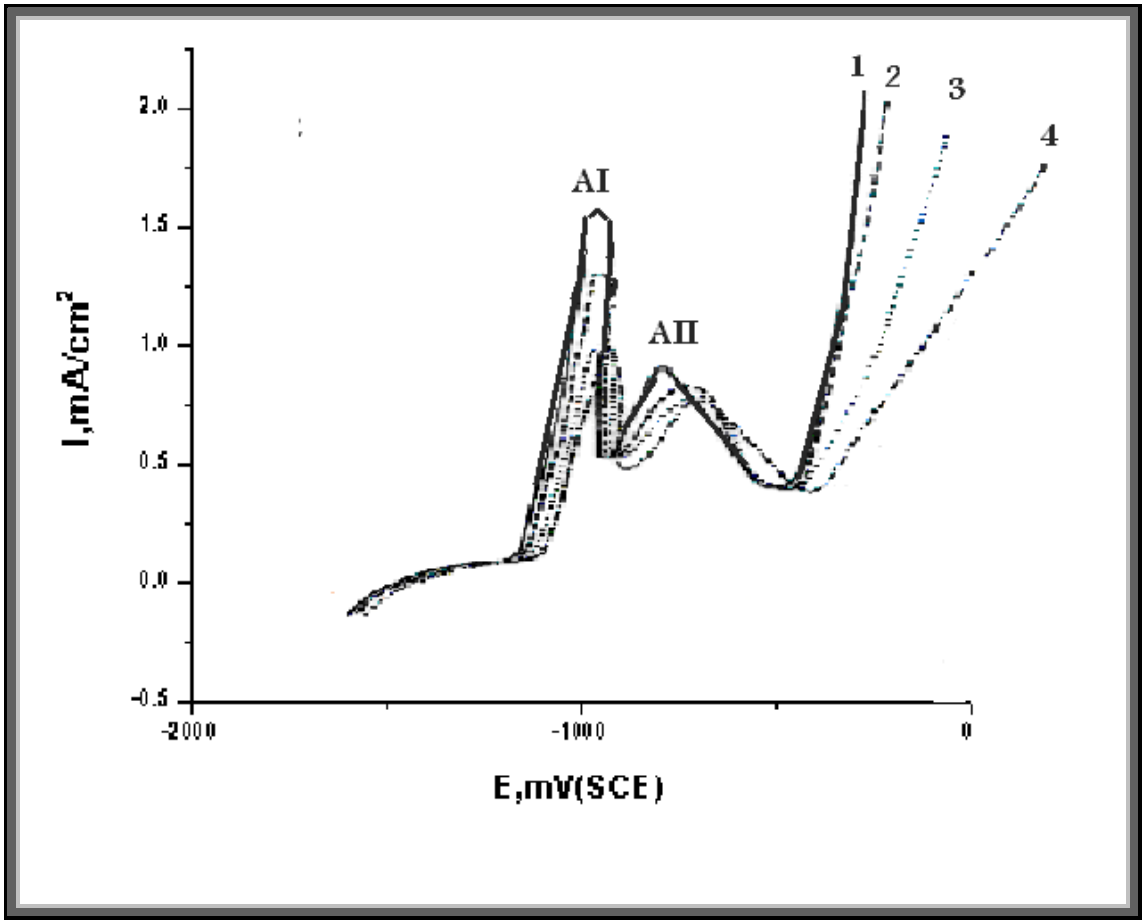

Fig.(3.7): Anodic cyclic voltammograms for tin electrode in various concentrations of NaCl solution at scan rate100 mV/sec. (1) 0.6, (2) 0.4, (3) 0.3 and (4) 0.2 M.

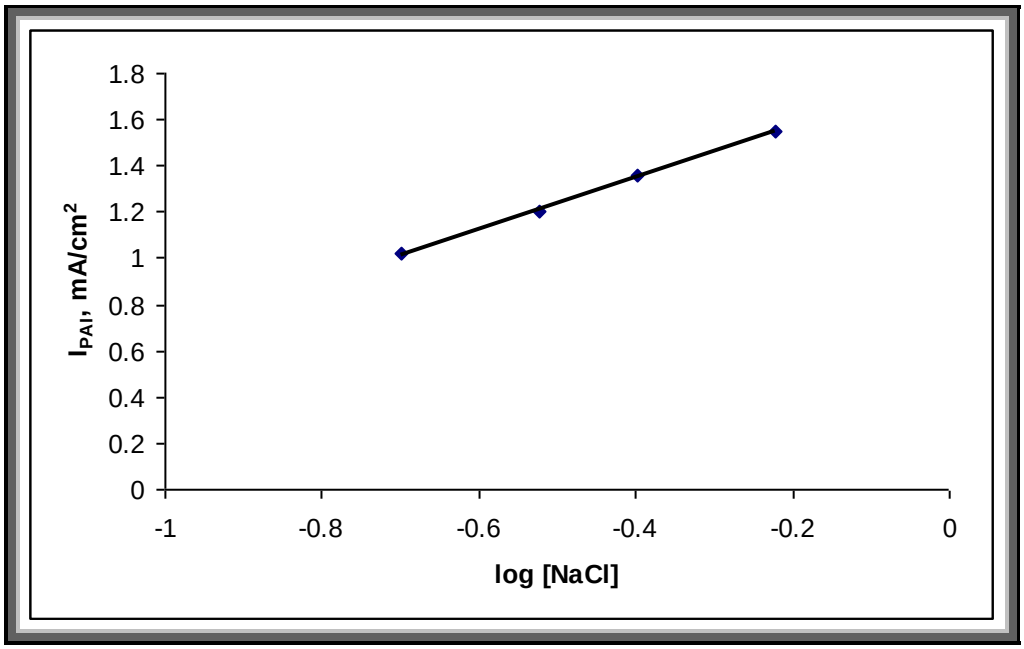

Fig.(3.8): The relation between (I_{PAI}) versus log [NaCl] for tin electrode at scan rate 100 mV/sec.

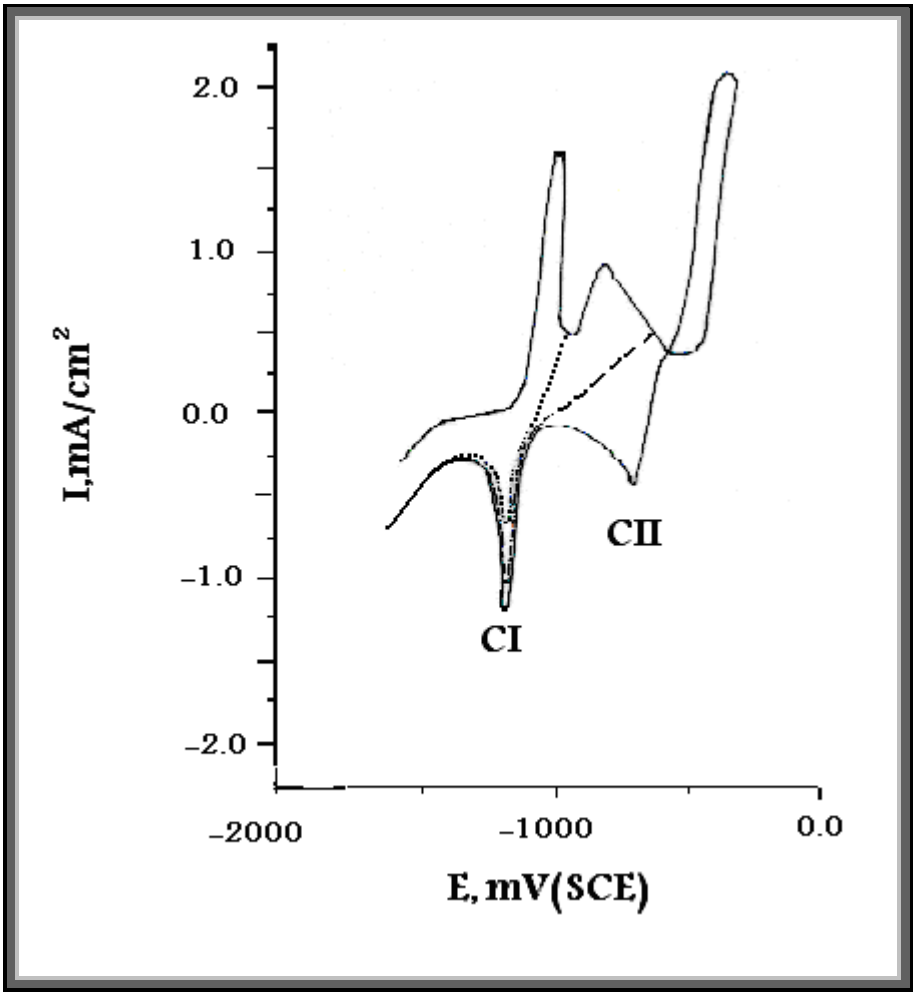

Fig.(3.9): Cyclic voltammograms for tin electrode in 0.6 M NaCl solution at scan rate 100 mV/sec, starting from -2000 mV and reversed at various anodic potential limits.

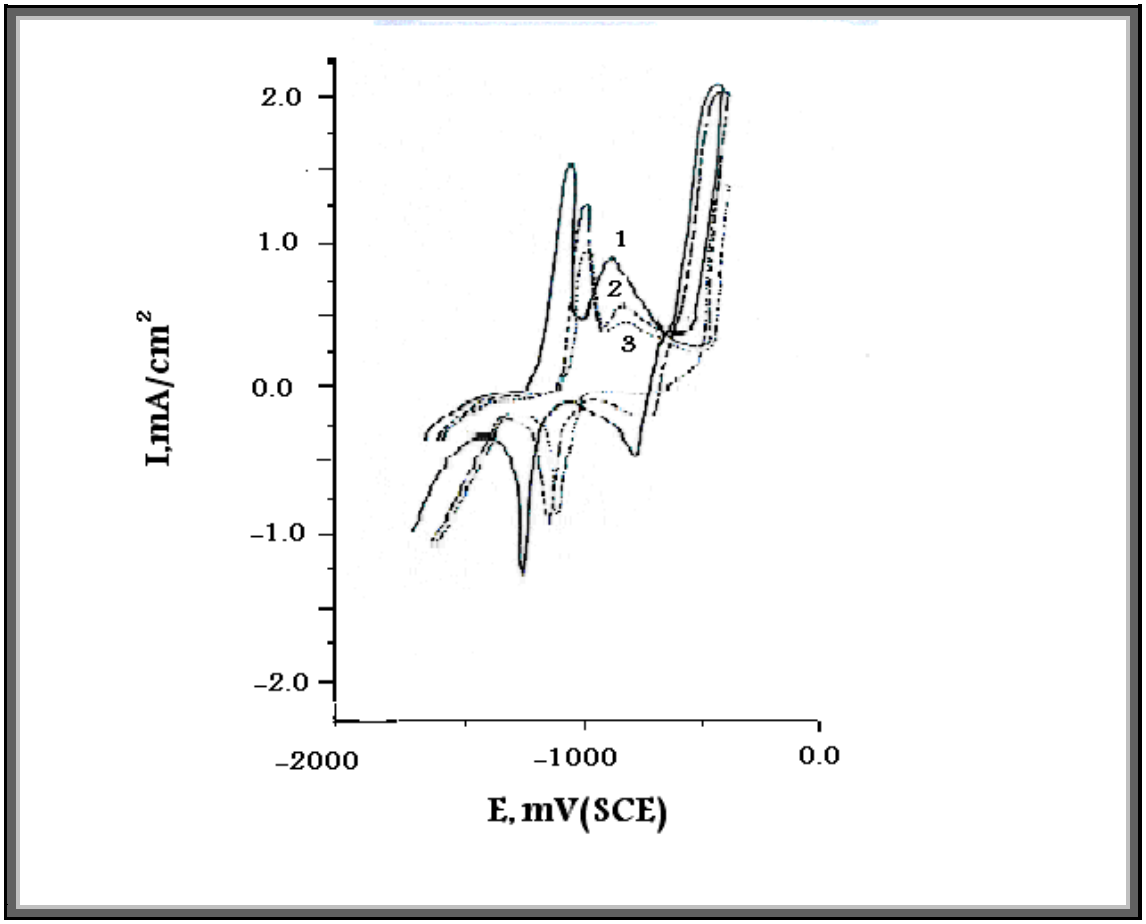

Fig.(3.10): Successive cyclic voltammograms for tin electrode in 0.6 M NaCl solution at scan rate 100 mV/sec.

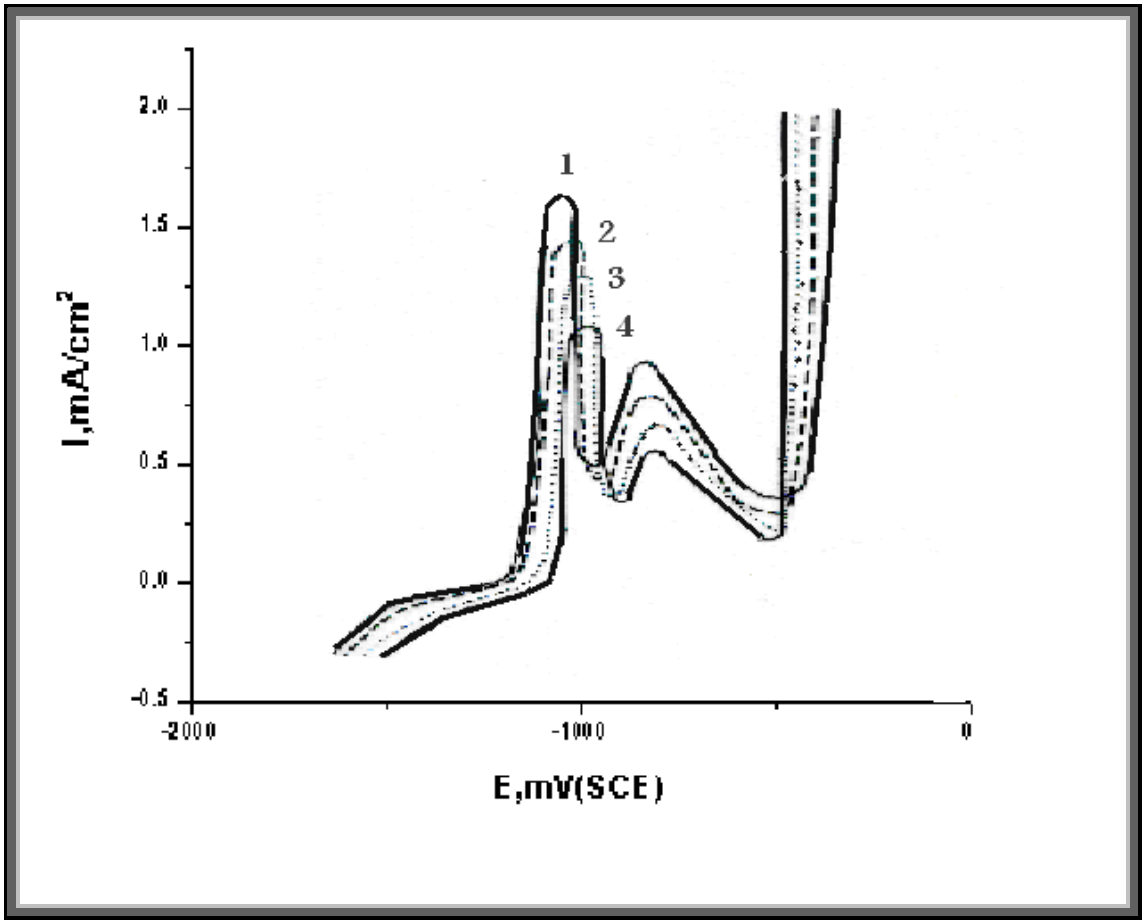

Fig.(3.11): Anodic cyclic voltammograms for tin electrode in 0.6 M NaCl solution at different scan rates (1) 100, (2) 75, (3) 50 and (4) 25 mV/sec.

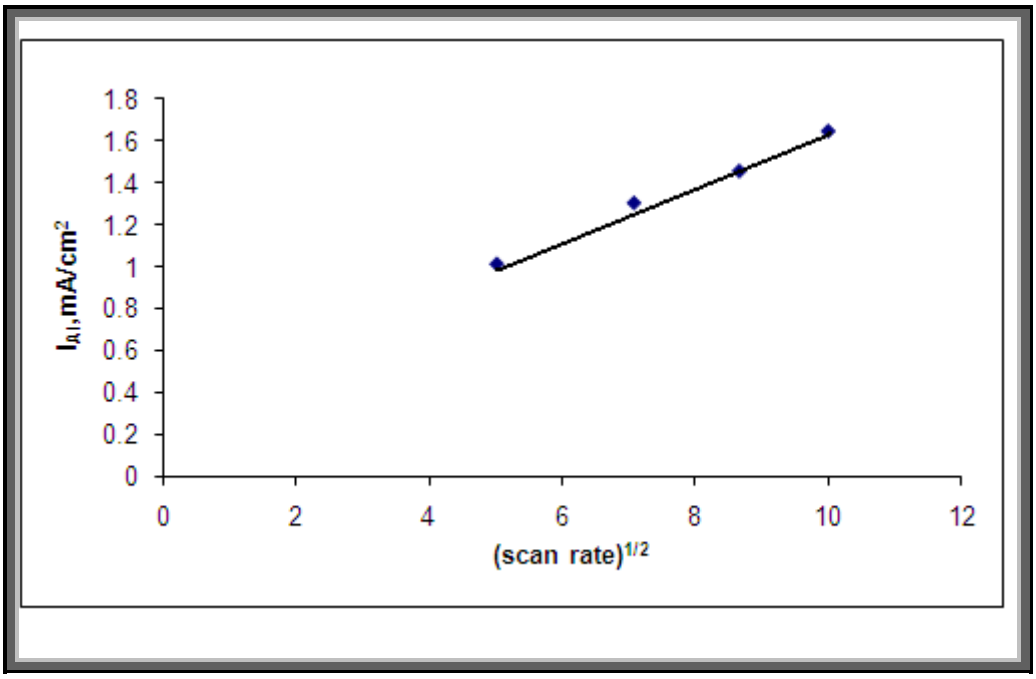

Fig.(3.12): Relation between I_{PAI} and (scan rate)$^{1/2}$ for tin electrode in 0.6 M NaCl solution.

Section (2)

Studying the corrosion inhibition of tin in $NaHCO_3$ and NaCl solutions by Galvanostatic polarization technique

3.2.1 Introduction.

The technique of anodic and cathodic polarization of metals is frequently used to study the phenomena of metal corrosion and passivation. It yields useful information on the electrode behavior, action of inhibitive and aggressive anions and the effect of the environmental condition. In this technique, an external applied electric current is used and can be varied at will; the experiment can be performed in relatively short time. When a Tafel equation is applicable for both anodic and cathodic polarization, the point of intersection of the two Tafel lines corresponding to the stationary conditions of corrosion. The function of a substance as an inhibitor or stimulator may thus be due to its effect on polarization curves, and consequent displacement of the point of intersection.

The extrapolation of anodic and/or cathodic Tafel lines of charge transfer controlled corrosion reaction gives the corrosion current density, I_{corr}, at the corrosion potential, E_{corr}. This method is based on the electrochemical theory of corrosion processes developed by Wagner and Traud [118]. Corrosion rates are determined through polarization curves. Polarization curves are produced through the application of a current to the metal surface. If the potential of the metal surface is polarized by the current in a positive sense it is referred to as being anodically polarized; a negative sense signifies that it is cathodically polarized. The degree of polarization is a measure of how the rates of the anodic and cathodic reactions are hindered by various environmental and surface process

factors. The environmental factors (the concentration of metal ions, dissolved oxygen in the solution, etc.) are referred to as the concentration polarization. The surface process factors (film formation, adsorption, etc.) are referred to as the activation polarization. The polatization curve is a graph of the variation of the potential as a function of the current, which allows the effects of the concentration and activation processes on the rate at which the anodic or cathodic reactions can give or receive electrons to be determined. This allows for a rate determination for the reactions that are involved in the corrosion process.

The polarization curves show the polarization curves for both anodic and cathodic reactions. The potential, E, is plotted as a function of logarithm of I_{corr}.

3.2.2 Galvanostatic polarization curves of tin electrode in $NaHCO_3$ solutions.

Figs. (3.13-3.15) represent the effect of addition of increasing concentrations of natural occurring substances e.g. lawsonia, licorice root and carob extracts, respectively, on the galvanostatic polarization curves of tin electrode in 0.1 M $NaHCO_3$ solution at scan rate 10 mV/sec.

Figs. (3.16-3.19) represent the effect of addition of increasing concentrations of some inorganic compounds such as sodium salts of CrO_4^{2-}, MoO_4^{2-}, WO_4^{2-} and HPO_4^{2-} ions, respectively, on the galvanostatic polarization curves of tin electrode in 0.1 M $NaHCO_3$ solution at scan rate 10 mV/sec.

Inspection of these figures revealed that, there is a transition region at the beginning of cathodic or anodic polarization known as pre-Tafel region. This region starts from the corrosion potential and extended to the

beginning of Tafel region. It is characterized by simultaneous occurrence of cathodic hydrogen evolution reaction and anodic dissolution of tin. The hydrogen evolution leads to cover a fraction (θ_H) of the electrode surface by the adsorbed hydrogen atoms $(MH)_{ads}$ and the anodic reaction causes a coverage of a fraction (θ_{OH}) of the same electrode by the adsorbed OH^- groups $(MOH)_{ads}$. These two reactions are in competition and hence give rise to mixed kinetics. Mc Cafferty et al. [119] and others [120-121] considered that, at the corrosion potential almost the whole electrode surface is covered by $(MH)_{ads}$ and consequently the coverage fraction (θ_H) is closed to unity at cathodic potentials and decrease when anodic polarization is increased. At the end of transition region there is a metal dissolution, in case of anodic polarization, and the current becomes purely anodic. In case of cathodic polarization the current becomes purely cathodic due to the hydrogen evolution reaction.

Further inspection of the curves of Figs.(3.13-3.19) reveal that, the presence of increasing concentrations of these compounds cause a decrease in the rate of anodic dissolution reaction. This may be ascribed to a parallel adsorption of the additives compounds over the corroding surface.

The percentage inhibition efficiency %IE imparted by the added inhibitor, which is defined as the percentage of the relative decrease in corrosion rate brought about by the presence of a certain concentration of the inhibitor is given by:

$$\%IE = [1 - (I_{add}/I_{free})] \times 100 \qquad (3.11)$$

where, I_{free} and I_{add} are the corrosion current densities in the absence and presence of the inhibitors, respectively.

The degree of surface coverage (θ) was calculated using the following equation:

$$\theta = 1 - (I_{add}/I_{free}) \quad (3.12)$$

where, I_{free} and I_{add} are defined before.

Tables (3.1-3.3) show the effect of increasing concentrations of some natural occurring substances e.g. lawsonia, licorice root and carob extracts, respectively, on some electrochemical parameters e.g. current density (I_{corr}), corrosion potential (E_{corr}) anodic and cathodic Tafel slopes (β_a and β_c), the degree of surface coverage (θ) and the percentage of inhibition efficiency (%IE) during corrosion of tin electrode in 0.1 M $NaHCO_3$ solution. Also Tables (3.4-3.7) show the effect of increasing concentrations of CrO_4^{2-}, MoO_4^{2-}, WO_4^{2-} and HPO_4^{2-} ions, respectively, on the same electrochemical parameters during the corrosion of tin electrode in 0.1 M $NaHCO_3$ solution.

Inspection of these Tables:

1- The corrosion potential (E_{corr}) values were shifted to more negative values by increasing the concentrations of the inhibitors.

2- The value of corrosion current density (I_{corr}) decreases and the inhibition efficiency (%IE) increases with increasing the concentration of the inhibitors, indicating the inhibiting effect of these compounds toward the dissolution of tin electrode in 0.1 M $NaHCO_3$ solution.

3- At one and the same concentration of the inhibitors, the order of inhibition efficiency of the plants extracts decreases in the following order:

Licorice root > Lawsonia > Carob

4- At one and the same concentration of the inhibitors, the order of inhibition efficiency of the inorganic compounds decreases in the following order:

$$CrO_4^{2-} > WO_4^{2-} > MoO_4^{2-} > HPO_4^{2-}$$

3.2.3 Adsorption isotherm.

The adsorption behavior of the additives (organic or inorganic) compounds on the metal surface can be interpreted by finding a suitable isotherm which describes the variation of experimentally obtained values of the amounts of adsorbed substances by unit area of the metal surface with its concentration in the bulk solution at constant temperature.

The additives compounds inhibit the corrosion process by adsorption on metal surface. Theoretically, the adsorption process can be regarded as a single substitutional process in which an inhibitor molecule, I, in the aqueous phase substitutes an "x" number of water molecules adsorbed on the metal surface, equation (1.2) . The adsorption depends on the structure of the inhibitor, the type of the metal and the nature of its surface, the nature of the corrosion medium, the pH value, the temperature and the electrochemical potential of the metal solution interface. Also, the adsorption provides information about the interaction among the adsorbed molecules themselves as well as their interaction with the metal surface. Actually an adsorbed molecule may make the surface more difficult or less difficult for another molecule to become attached to a neighboring site and multilayer adsorption may take place. There may be more or less than one inhibitor molecule per surface site. Finally, various surface sites could have varying degree of activation. For these reasons a number of mathematical adsorption isotherm expressions have been developed, as has been mentioned in chapter 1.

A number of mathematical relationships for the adsorption isotherms have been suggested to fit the experimental data of the present work. The equation that fits our results is that due to Freundlich isotherm [50] and is given by the general equation:

$$\theta = K.C^n \qquad (1.9)$$

or alternatively by:

$$\log \theta = \log K + n \log C \qquad (3.13)$$

where K and C are the equilibrium constant of adsorption process and additives concentrations, respectively.

A plot log θ against log C gives a straight line of intercept, log K, these plots are shown for all compounds used in Figs. (3.20-3.21).
Linear correlations are obtained for all compounds suggesting that the Freundlich adsorption isotherm is obeyed. The calculated values for the equilibrium constant of adsorption were listed in Table (3.8).

The equilibrium constant of adsorption K is related to the standard free energy of adsorption, equation (1.11).

The values of ΔG^o_{ads} were calculated and listed in Table (3.8). The standard free energy change of adsorption is associated with water adsorption/desorption equilibrium which forms an important part in the overall free energy changes of adsorption. It is clear that ΔG^o_{ads} increases with the increase of solution energy of adsorption species [9]. The negative values of ΔG^o_{ads} obtained have indicated that the adsorption process of these compounds on the metal surface is spontaneous one.

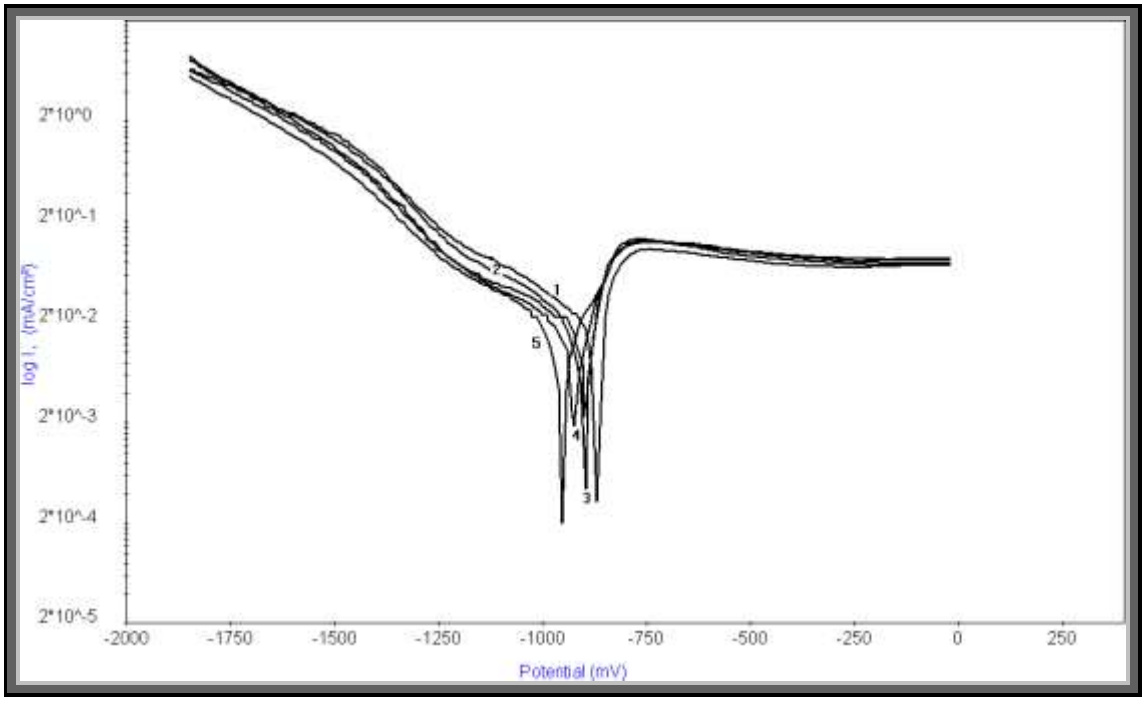

Fig.(3.13): Anodic and cathodic polarization curves for tin electrode in 0.1 M $NaHCO_3$ solution in presence of different concentrations of lawsonia extract at scan rate 10 mV/sec. (1) 0, (2) 500, (3) 1000, (4) 1500 and (5) 1600 ppm.

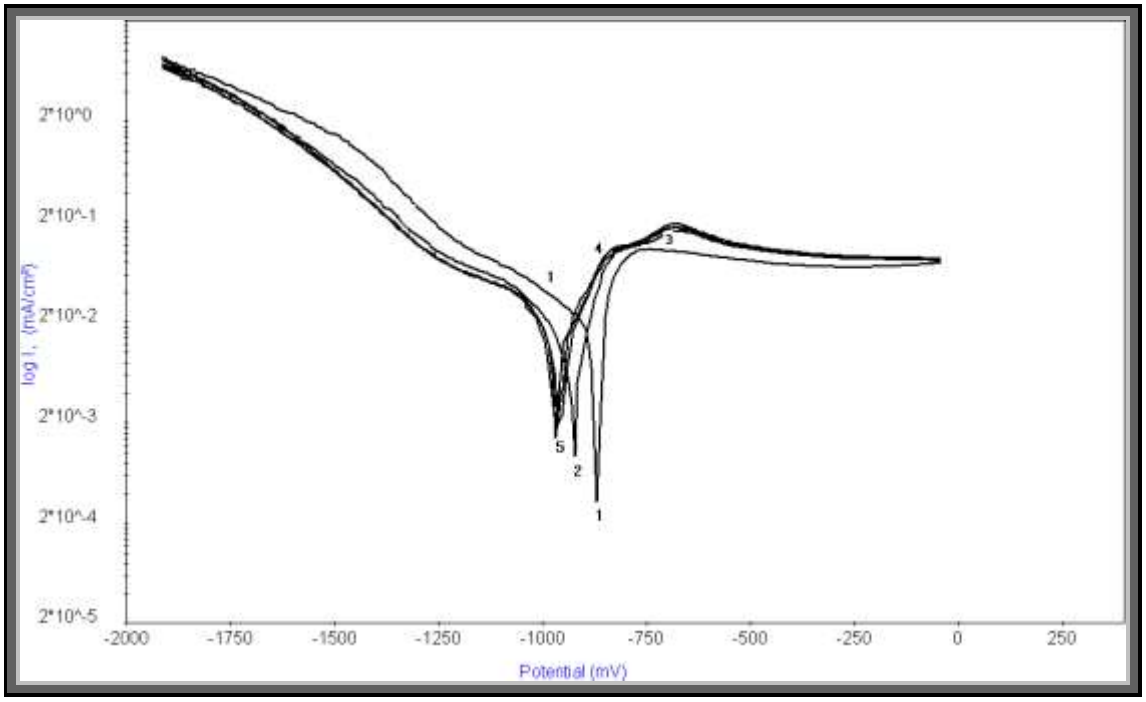

Fig.(3.14): Anodic and cathodic polarization curves for tin electrode in 0.1 M $NaHCO_3$ solution in presence of different concentrations of licorice root extract at scan rate 10 mV/sec. (1) 0, (2) 500, (3) 1000, (4) 1500 and (5) 2500 ppm.

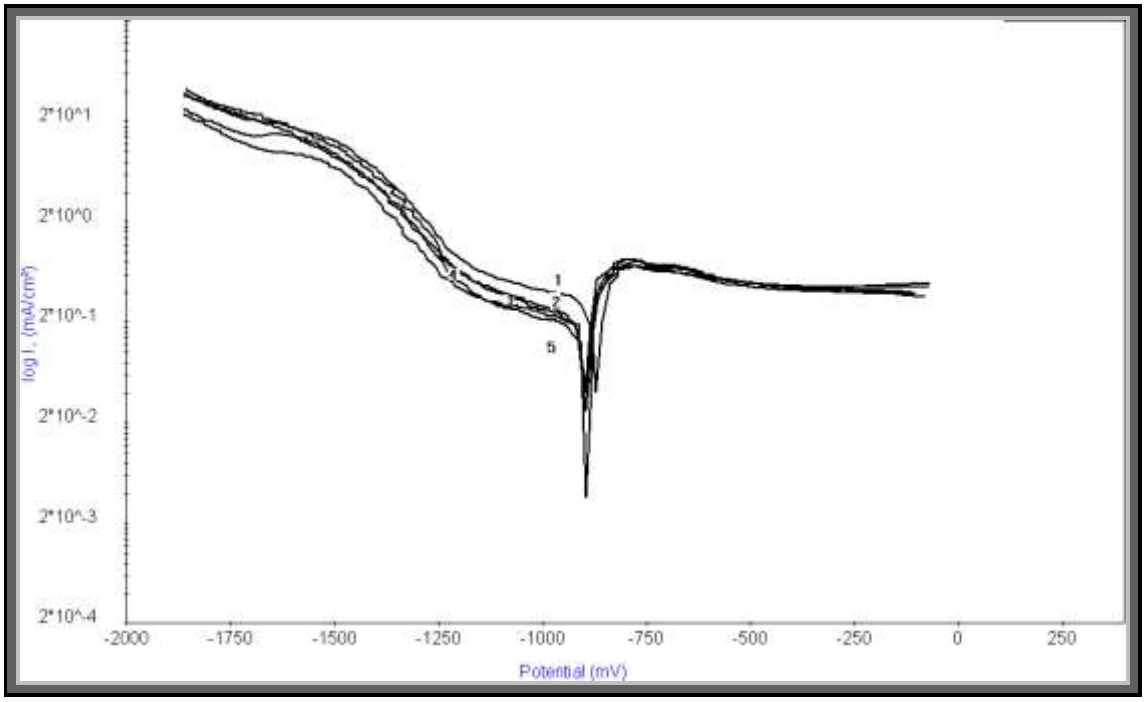

Fig.(3.15): Anodic and cathodic polarization curves for tin electrode in 0.1 M $NaHCO_3$ solution in presence of different concentrations of carob extract at scan rate 10 mV/sec. (1) 0, (2) 500, (3) 1000, (4) 2000 and (5) 3000 ppm.

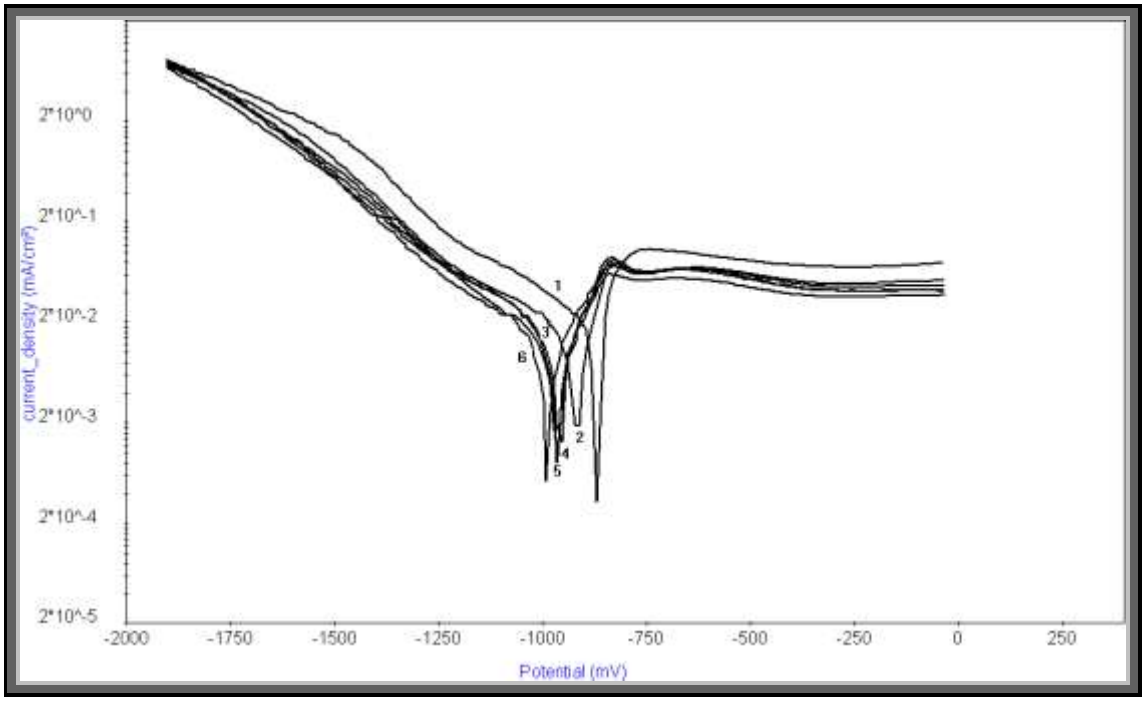

Fig.(3.16): Anodic and cathodic polarization curves for tin electrode in 0.1 M $NaHCO_3$ solution in presence of different concentrations of CrO_4^{2-} ions at scan rate 10 mV/sec. (1) 0, (2) 0.004, (3) 0.006, (4) 0.008, (5) 0.01 and (6)0.012 M.

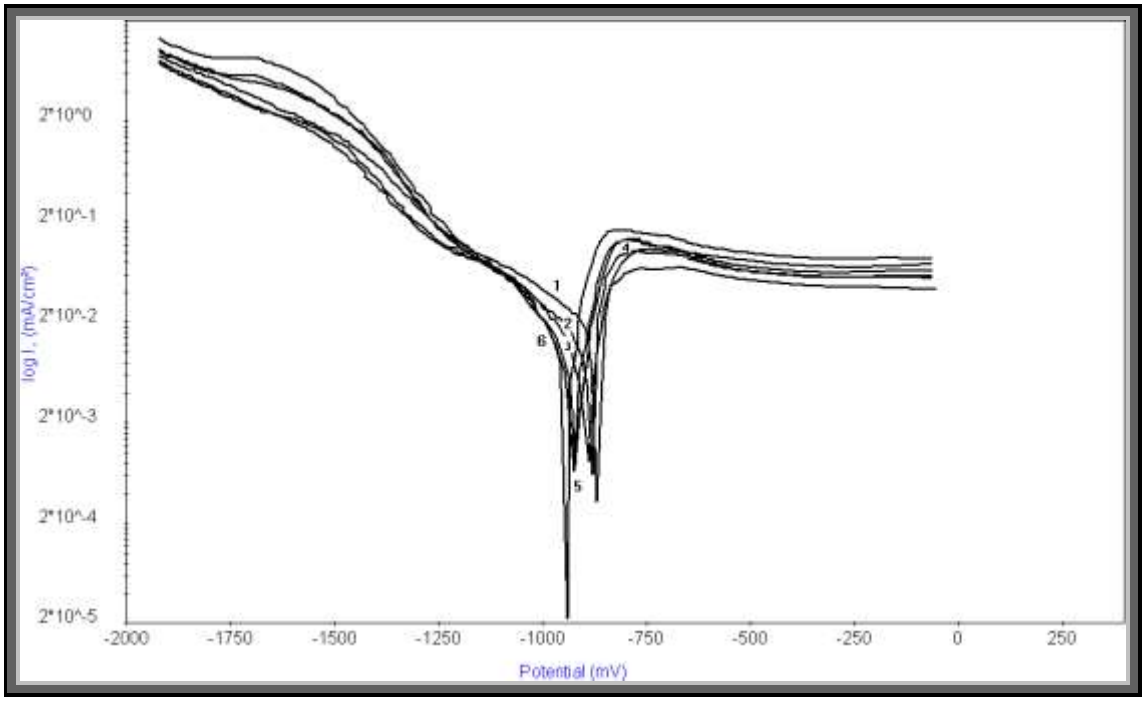

Fig.(3.17): Anodic and cathodic polarization curves for tin electrode in 0.1 M $NaHCO_3$ solution in presence of different concentrations of MoO_4^{2-} ions at scan rate 10 mV/sec. (1) 0, (2) 0.01, (3) 0.02, (4) 0.03, (5) 0.04 and (6) 0.05 M.

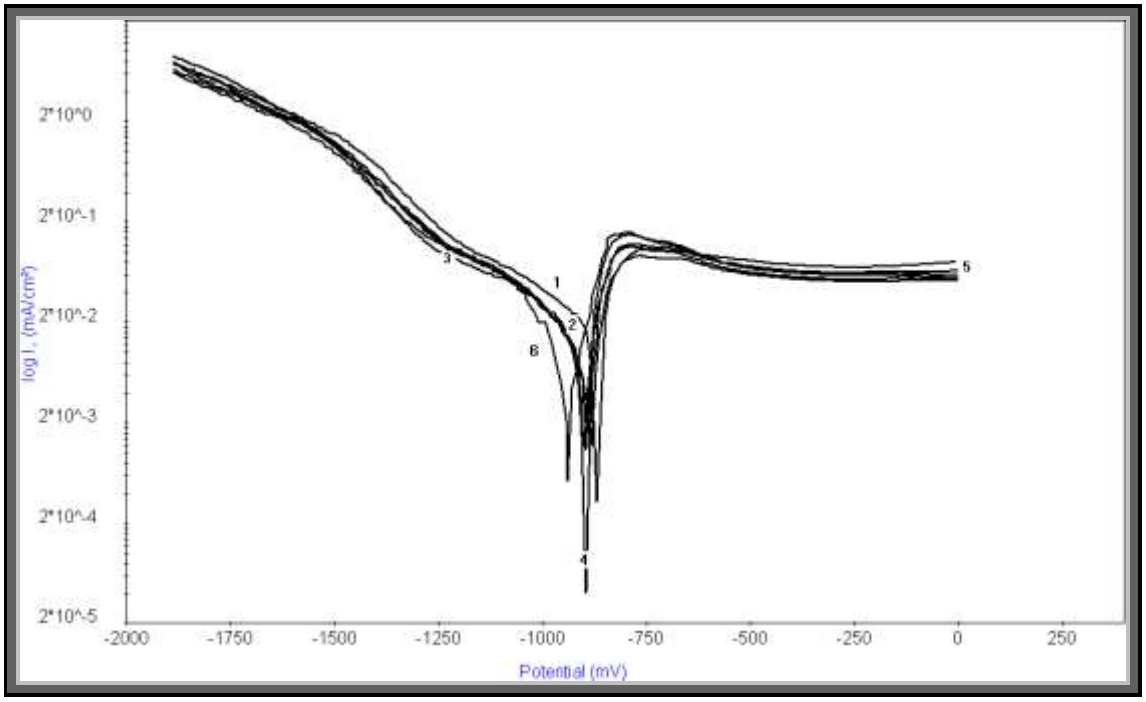

Fig.(3.18): Anodic and cathodic polarization curves for tin electrode in 0.1 M $NaHCO_3$ solution in presence of different concentrations of WO_4^{2-} ions at scan rate 10 mV/sec. (1) 0, (2) 0.01, (3) 0.02, (4) 0.025, (5) 0.035 and (6) 0.04 M.

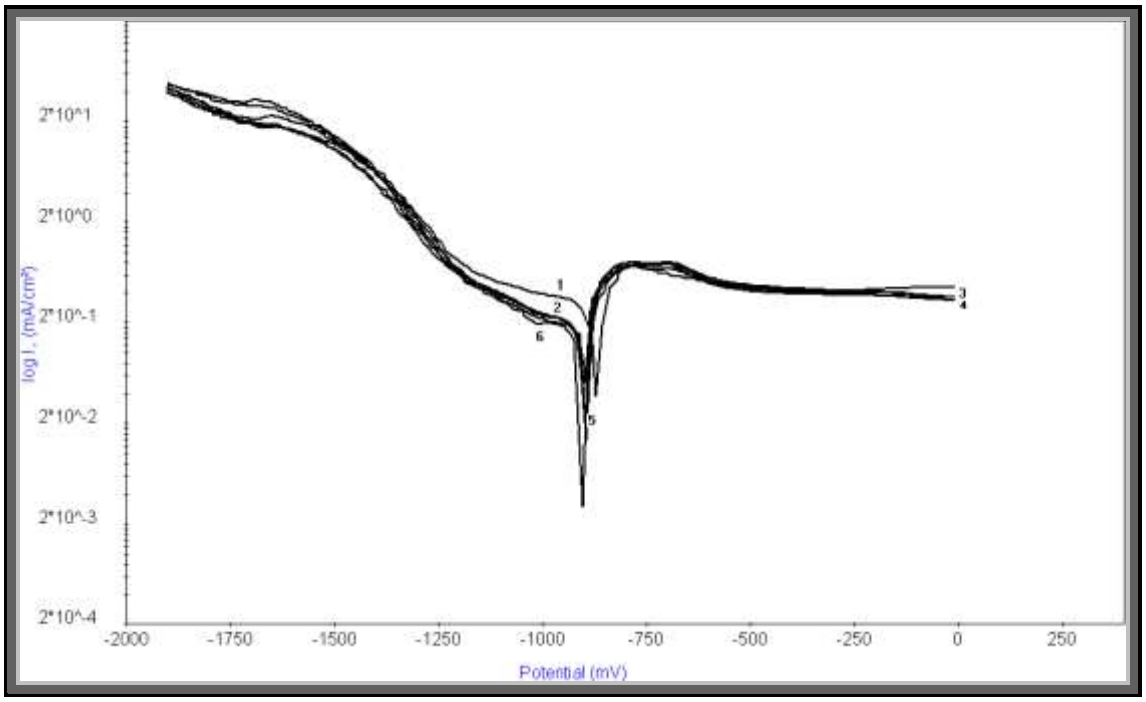

Fig.(3.19): Anodic and cathodic polarization curves for tin electrode in 0.1 M $NaHCO_3$ solution in presence of different concentrations of HPO_4^{2-} ions at scan rate 10 mV/sec. (1) 0, (2) 0.01, (3) 0.04, (4) 0.05, (5) 0.055 and (6) 0.06 M.

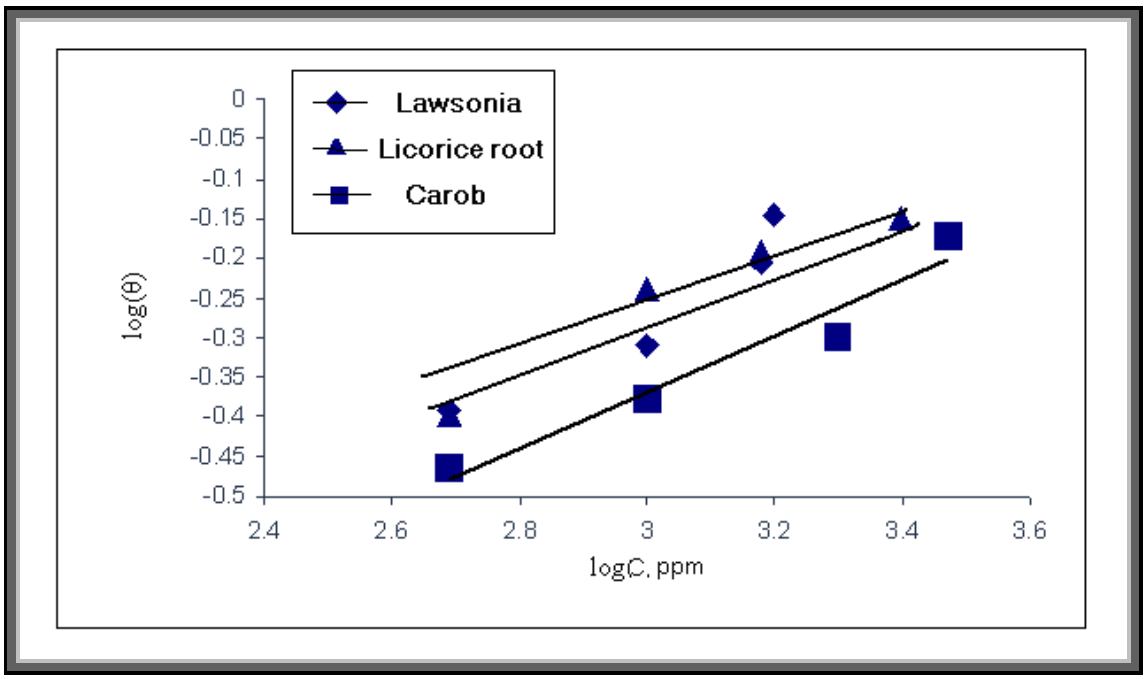

Fig.(3.20): The relation between log (θ) and log C, ppm for tin electrode in 0.1 M $NaHCO_3$.

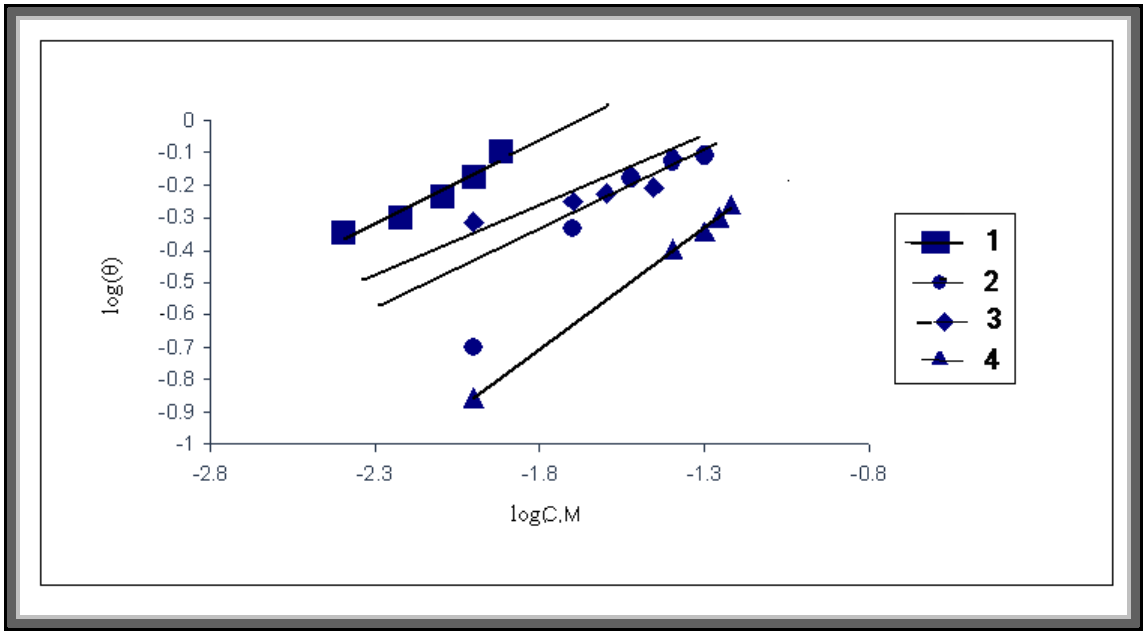

Fig.(3.21): The relation between log (θ) and log C, M for tin electrode in 0.1 M $NaHCO_3$, where: 1) CrO_4^{2-} 2) MoO_4^{2-} 3) WO_4^{2-} 4) HPO_4^{2-}.

Table (3.1): Corrosion parameters obtained from galvanostatic polarization measurements of tin electrode in 0.1 M $NaHCO_3$ solution containing different concentrations of lawsonia extract.

Inh. conc. (ppm)	**β_a mV. dec^{-1}**	**β_a mV. dec^{-1}**	**E_{corr} mV (SCE)**	**I_{corr} µA/cm^2**	**θ**	**%IE**
0	119.45	-336.46	-868	7.843	-	-
500	70.02	-255.62	-889	4.655	0.4064	40.64
1000	74.04	-173.73	-896	3.997	0.4904	49.04
1500	84.73	-142.54	-923	2.969	0.6214	62.14
1600	84.35	-121.34	-952	2.245	0.7138	71.38

Table (3.2): Corrosion parameters obtained from galvanostatic polarization measurements of tin electrode in 0.1 M $NaHCO_3$ solution containing different concentrations of licorice root extract.

Inh. conc. (ppm)	**β_a mV. dec^{-1}**	**β_c mV. dec^{-1}**	**E_{corr} mV (SCE)**	**I_{corr} µA/cm^2**	**θ**	**%IE**
0	119.45	-336.46	-868	7.843	-	-
500	119.90	-177.96	-968	4.702	0.4004	40.04
1000	76.72	-160.28	-967	3.334	0.5749	57.49
1500	71.47	-143.91	-963	2.95	0.6238	62.38
2500	66.46	-112.97	-920	2.709	0.6545	65.45

Table (3.3): Corrosion parameters obtained from galvanostatic polarization measurements of tin electrode in 0.1 M $NaHCO_3$ solution containing different concentrations of carob extract.

Inh. conc. (ppm)	**β_a mV. dec^{-1}**	**β_c mV. dec^{-1}**	**E_{corr} mV (SCE)**	**I_{corr} µA/cm^2**	**θ**	**%IE**
0	119.45	-336.46	-868	7.843	-	-
500	82.08	-220.85	-894	5.157	0.3425	34.25
1000	73.79	-203.13	- 895	4.556	0.4191	41.91
2000	76.02	-162.58	-895	3.912	0.5012	50.12
3000	57.97	-111.20	-895	2.560	0.6736	67.36

Table (3.4): Corrosion parameters obtained from galvanostatic polarization measurements of tin electrode in 0.1 M $NaHCO_3$ solution containing different concentrations of CrO_4^{2-} ions.

Inh. conc. (M)	**β_a mV. dec^{-1}**	**β_c mV. dec^{-1}**	**E_{corr} mV (SCE)**	**I_{corr} µA/cm^2**	**θ**	**%IE**
0	119.45	-336.46	-868	7.843	-	-
0.004	57.24	-408.43	-911	4.292	0.4528	45.28
0.006	80.36	-334.84	-953	3.925	0.4996	49.96
0.008	93	-283.73	-962	3.263	0.5840	58.40
0.01	87.13	-176.17	-966	2.569	0.6724	67.24
0.012	100.50	-75.45	-991	1.545	0.8030	80.30

Table (3.5): Corrosion parameters obtained from galvanostatic polarization measurements of tin electrode in 0.1 M $NaHCO_3$ solution containing different concentrations of MoO_4^{2-} ions.

Inh. conc. (M)	**β_a mV. dec^{-1}**	**β_c mV. dec^{-1}**	**E_{corr} mV (SCE)**	**I_{corr} µA/cm^2**	**θ**	**%IE**
0	119.45	-336.46	-868	7.843	-	-
0.01	172.68	-255.35	-888	6.285	0.1986	19.86
0.02	86.16	-253.20	-920	4.242	0.4591	45.91
0.03	79.41	-164.02	-924	2.606	0.6677	66.77
0.04	58.83	-122.23	-924	1.995	0.7456	74.56
0.05	58.81	-104.50	-926	1.693	0.7841	78.41

Table (3.6): Corrosion parameters obtained from galvanostatic polarization measurements of tin electrode in 0.1 M $NaHCO_3$ solution containing different concentrations of WO_4^{2-} ions.

Inh. conc. (M)	**β_a mV. dec^{-1}**	**β_c mV. dec^{-1}**	**E_{corr} mV (SCE)**	**I_{corr} µA/cm^2**	**θ**	**%IE**
0	119.45	-336.46	-868	7.843	-	-
0.01	73.47	-268.37	-883	4.049	0.4837	48.37
0.02	54.32	-233.97	-902	3.436	0.5619	56.19
0.025	56.51	-206.91	-895	3.181	0.5944	59.44
0.035	53.59	-169.73	-896	2.977	0.6204	62.04
0.04	51.62	-125.55	-940	1.812	0.7690	76.90

Table (3.7): Corrosion parameters obtained from galvanostatic polarization measurements of tin electrode in 0.1 M $NaHCO_3$ solution containing different concentrations of HPO_4^{2-} ions.

Inh. conc. (M)	**β_a mV. dec^{-1}**	**β_c mV. dec^{-1}**	**E_{corr} mV (SCE)**	**I_{corr} µA/cm^2**	**θ**	**%IE**
0	119.45	-336.46	-868	7.843	-	-
0.01	112.56	-287.18	-876	6.754	0.1388	13.88
0.04	89.05	193.72	-895	4.703	0.4004	40.04
0.05	69.77	201.56	-903	4.267	0.4559	45.59
0.055	72.17	171.74	-897	3.902	0.5025	50.25
0.06	69.67	162.06	-905	3.552	0.5471	54.71

Table (3.8): Equilibrium constant and the adsorption free energy of the inhibitors adsorbed on the surface of tin electrode in 0.1 M $NaHCO_3$.

Inhibitor type	**K**	**ΔG^{o}_{ads} Cal. mol^{-1}**
Lawsonia	0.026	-93.3
Licorice root	0.047	-250.9
Carob	0.037	-189.6
CrO_4^{2-}	7.250	-1552.4
MoO_4^{2-}	12.380	-1690.8
WO_4^{2-}	1.720	-1180.3
HPO_4^{2-}	4.510	-1429.4

3.2.4 Galvanostatic polarization curves of tin electrode in NaCl solutions.

Figs. (3.22-3.24) represent the effect of addition of increasing concentrations of natural occurring substances e.g. lawsonia, licorice root and carob extracts, respectively, on the galvanostatic polarization curves of tin electrode in 0.6 M NaCl solution at scan rate 10 mV/sec.

Figs. (3.25-3.28) represent the effect of addition of increasing concentrations of some inorganic compounds such as CrO_4^{2-}, MoO_4^{2-}, WO_4^{2-} and HPO_4^{2-} ions, respectively, on the galvanostatic polarization curves of tin electrode in 0.6 M NaCl solution at scan rate 10 mV/sec.

Inspection of the curves of these figures, one can observe at first a transition region in which the potential increases (anodic polarization) or decreases (cathodic polarization) slowly with current density following the region there is a rapid linear build up of potential with current density (Tafel region).

Further inspection of the curves of Figs.(3.22-3.38) reveal that, the presence of increasing concentrations of these compounds cause a decrease in the rate of anodic dissolution reaction. This may be ascribed to a parallel adsorption of the organic molecules over the corroding surface.

The numerical values of the variation of corrosion current density (I_{corr}), corrosion potential (E_{corr}) anodic and cathodic Tafel slopes (β_a and β_c) , the degree of surface coverage (θ) and inhibition efficiency (%IE) with the concentrations of lawsonia, licorice root and carob extracts in 0.6 M NaCl solution, are given in Tables (3.9-3.11), respectively.

The numerical values of the variation of corrosion current density (I_{corr}), corrosion potential (E_{corr}) anodic and cathodic Tafel slopes (β_a and β_c) , the degree of surface coverage (θ) and inhibition efficiency (%IE) with the concentrations of CrO_4^{2-}, MoO_4^{2-}, WO_4^{2-} and HPO_4^{2-} ions in 0.6 M NaCl solution, are given in Tables (3.12-3.15), respectively.

Inspection of these Tables:

1- The corrosion potential (E_{corr}) values nearly constant.

2- The value of corrosion current density (I_{corr}) decreases and the inhibition efficiency (%IE) increases with increasing the concentration of the inhibitors, except MoO_4^{2-} ions, which indicating the inhibiting effect of these compounds toward the dissolution of tin electrode in 0.6 M NaCl solution.

3- It was found that MoO_4^{2-} ions accelerate the corrosion rate, which may be due to formation tin-oxy chloride, according to equation (3.10), which makes the solution acid. It was known that in acidic media the orthomolybdate ion, MoO_4^{2-}, condense into octamolybdate ion $Mo_8O_{26}^{4-}$ [122]. The steric effect may cause this acceleration.

4- At one and the same concentration of the inhibitors, the order of inhibition efficiency of the natural occurring substance decreases in the following order:

Lawsonia > Carob > Licorice root

5- At one and the same concentration of the inhibitors, the order of inhibition efficiency of the inorganic compounds decreases in the following order:

$$CrO_4^{2-} > HPO_4^{2-} > WO_4^{2-}$$

3.2.5 Adsorption isotherm.

The degree of surface coverage (θ) which represents the part of metal surface covered by inhibitor molecules was calculated using equation (3.12). The values of (θ) have been shown in Tables (3.9-3.15). The degree of surface coverage was found to increase with increasing concentration of additives. Attempts were made to fit θ values to various isotherms including Langmuir, Freundich, Temkin and Frumkin. By far, the best fit was obtained with Freundlich isotherm Figs. (3.29-3.30) represents the relation between log (θ) and log [Inhibitor]. Linear correlations are obtained for all compounds suggesting that the Freundlich adsorption isotherm is obeyed. The calculated values for the equilibrium constant of adsorption were listed in Table (3.16).

The values of ΔG^{o}_{ads} were calculated and listed in Table (3.16). The standard free energy change of adsorption is associated with water adsorption/desorption equilibrium which forms an important part in the overall free energy changes of adsorption. The negative values of ΔG^{o}_{ads} obtained have indicated that the adsorption process of these compounds on the metal surface is spontaneous one.

.

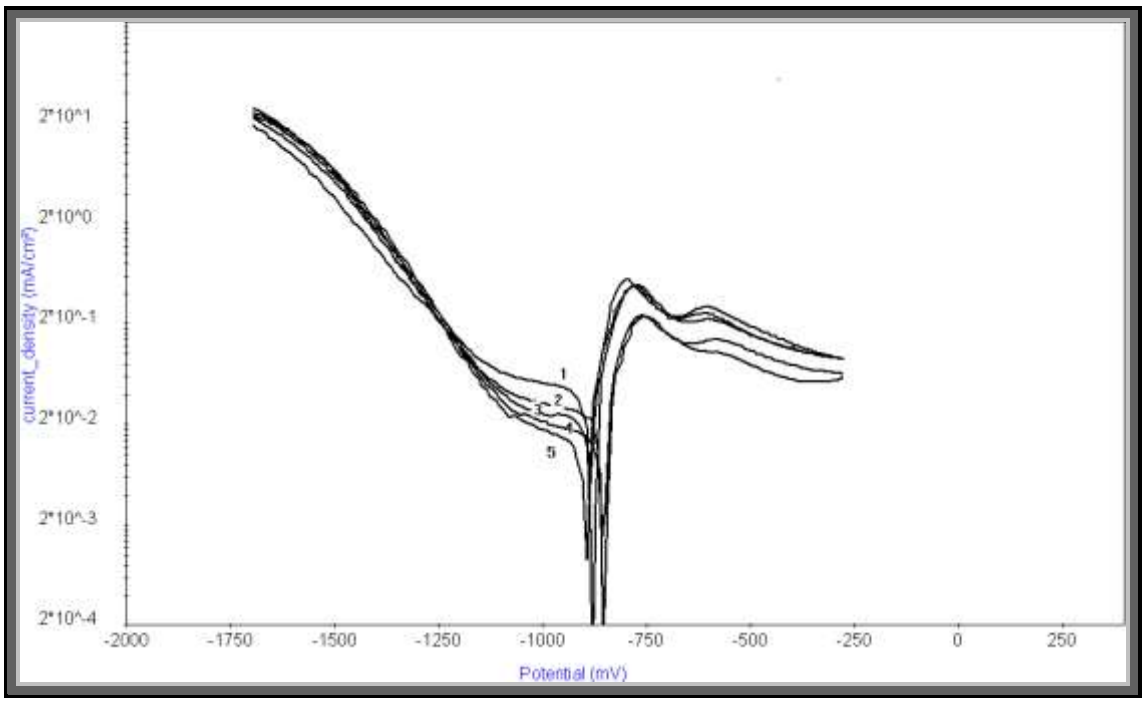

Fig.(3.22): Anodic and cathodic polarization curves for tin electrode in 0.6 M NaCl solution in presence of different concentrations of lawsonia extract at scan rate 10 mV/sec. (1) 0, (2) 1000, (3) 1500, (4) 2500 and (5) 3000 ppm.

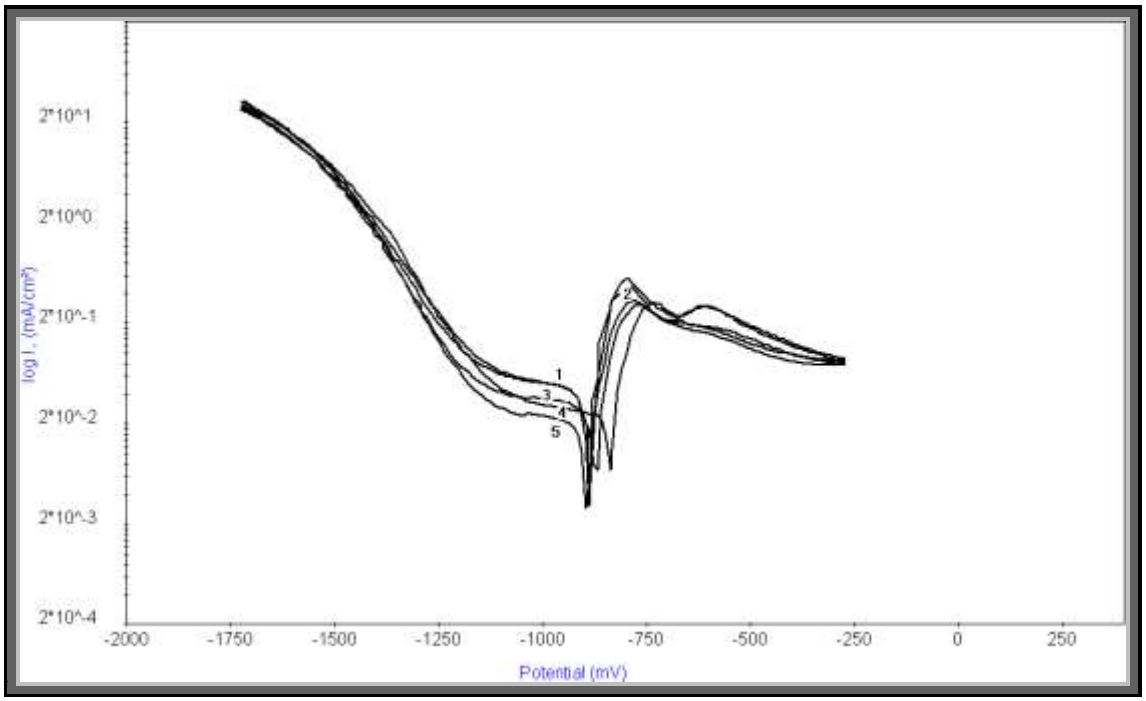

Fig.(3.23): Anodic and cathodic polarization curves for tin electrode in 0.6 M NaCl solution in presence of different concentrations of licorice root extract at scan rate 10 mV/sec. (1) 0, (2) 1000, (3) 2000, (4) 2500 and (5) 3000 ppm.

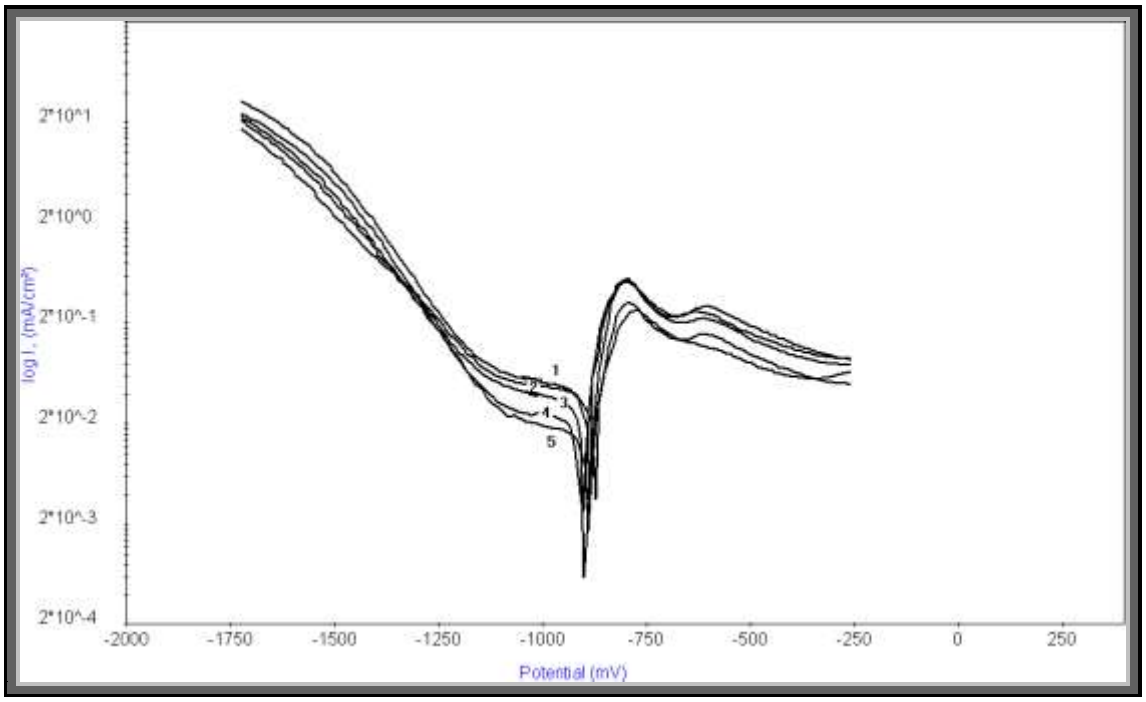

Fig.(3.24): Anodic and cathodic polarization curves for tin electrode in 0.6 M NaCl solution in presence of different concentrations of carob extract at scan rate 10 mV/sec. (1) 0, (2) 500, (3) 1000, (4) 2000 and (5) 3000 ppm.

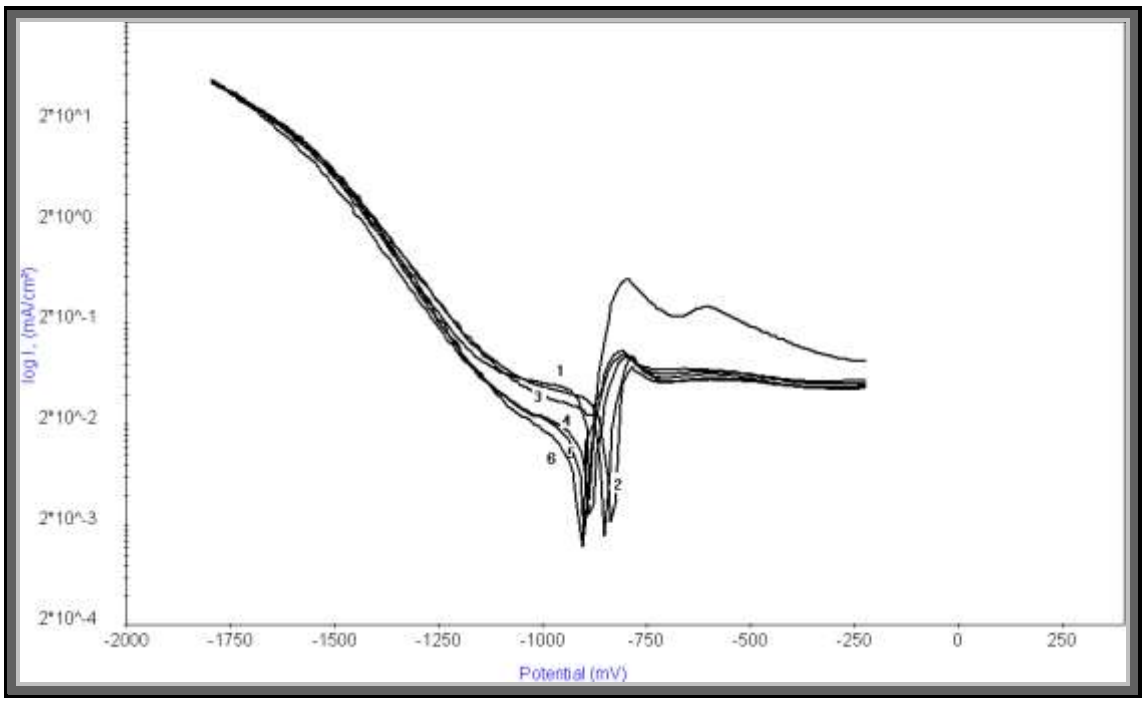

Fig.(3.25): Anodic and cathodic polarization curves for tin electrode in 0.6 M NaCl solution in presence of different concentrations of CrO_4^{2-} ions at scan rate 10 mV/sec. (1) 0, (2) 0.01, (3) 0.02, (4) 0.03, (5) 0.04 and (6) 0.05 M.

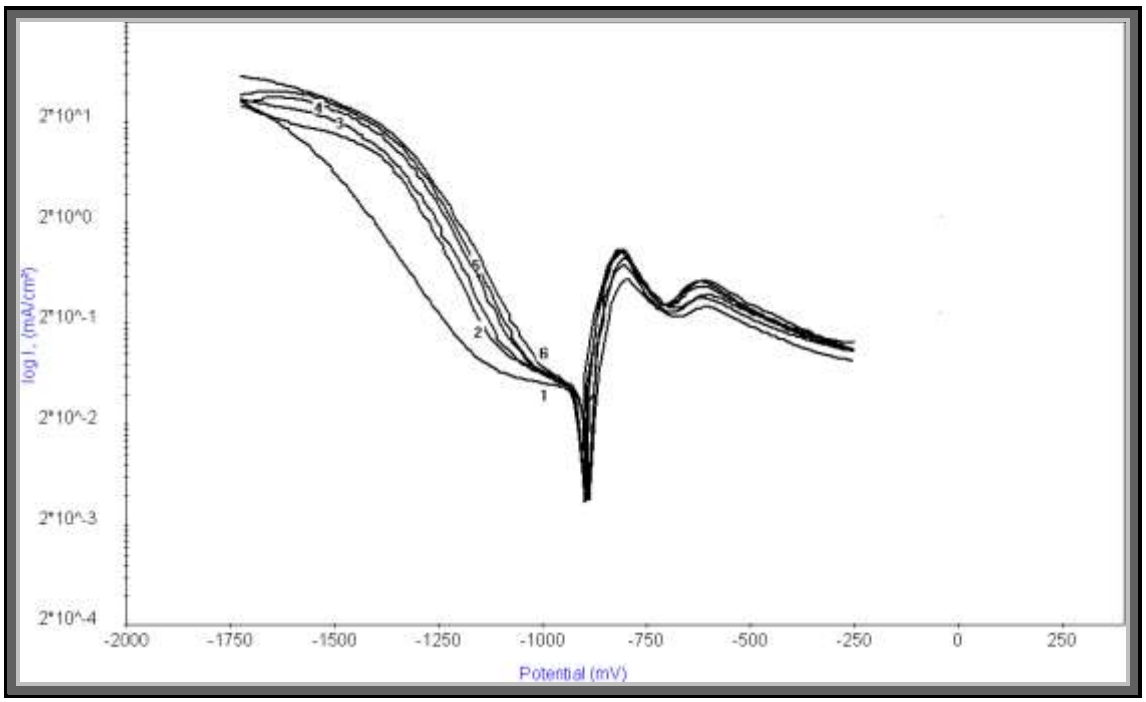

Fig.(3.26): Anodic and cathodic polarization curves for tin electrode in 0.6 M NaCl solution in presence of different concentrations of MoO_4^{2-} ions at scan rate 10 mV/sec. (1) 0, (2) 0.01, (3) 0.02, (4) 0.03, (5) 0.04, (6) 0.05 M.

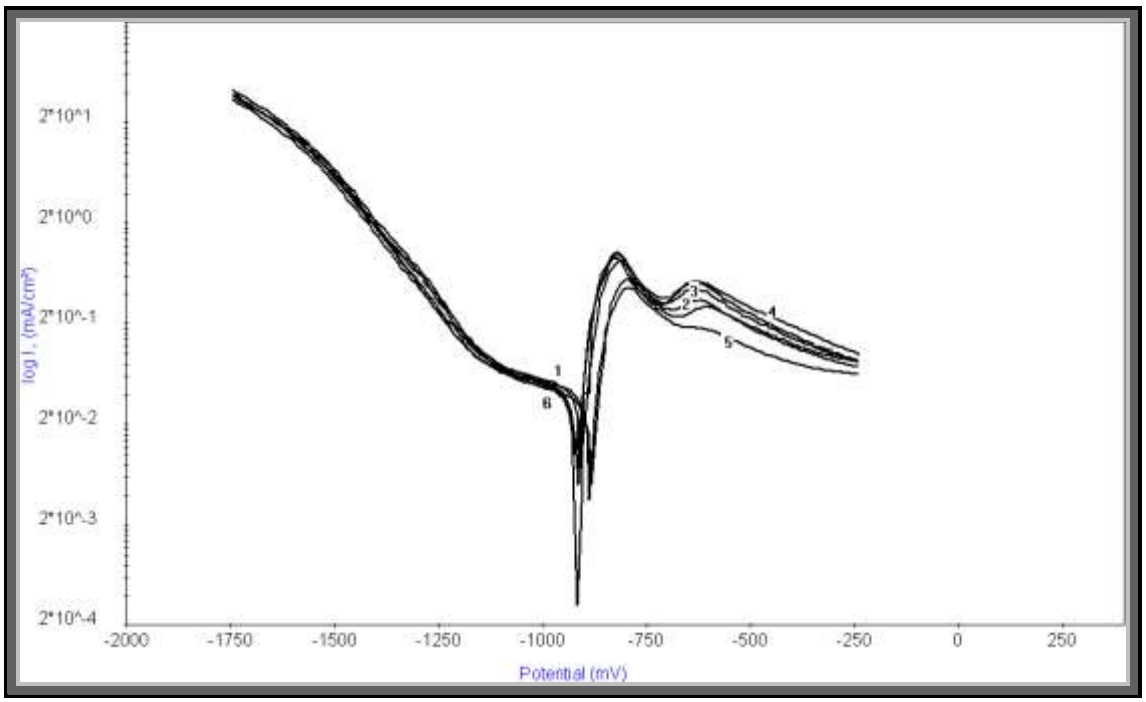

Fig.(3.27): Anodic and cathodic polarization curves for tin electrode in 0.6 M NaCl solution in presence of different concentrations of WO_4^{2-} ions at scan rate 10 mV/sec. (1) 0, (2) 0.03, (3) 0.06, (4) 0.1, (5) 0.12 and (6) 0.14 M.

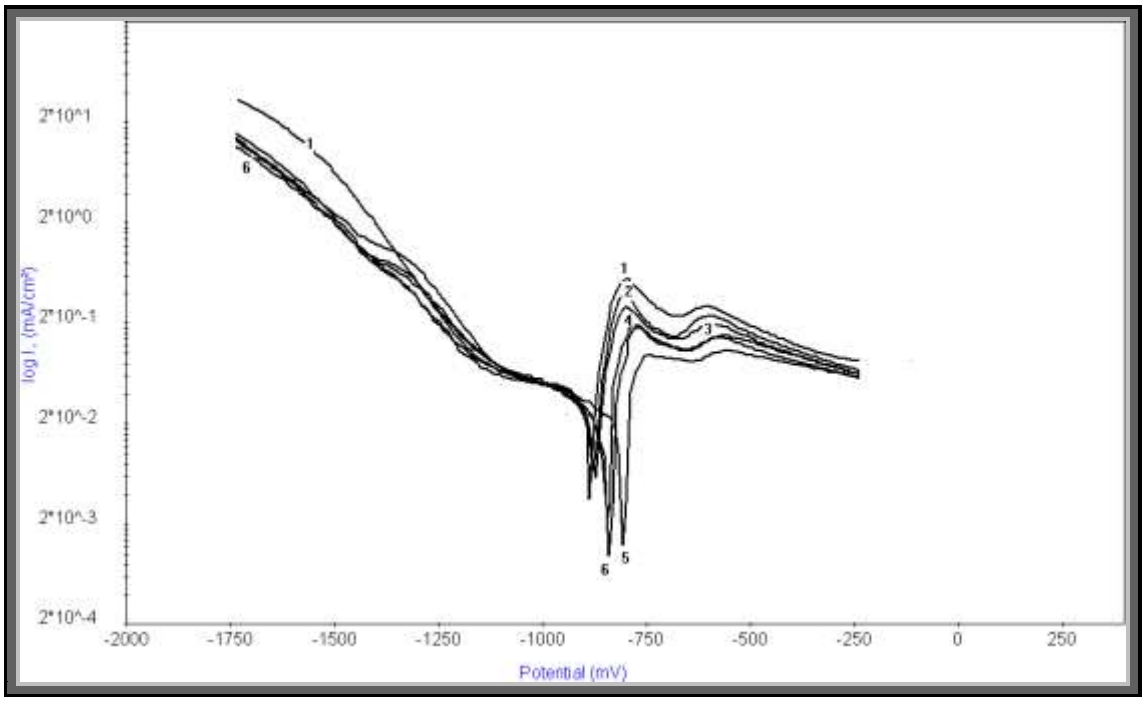

Fig.(3.28): Anodic and cathodic polarization curves for tin electrode in 0.6 M NaCl solution in presence of different concentrations of HPO_4^{2-} ions at scan rate 10 mV/sec. (1) 0, (2) 0.005, (3) 0.01, (4) 0.02, (5) 0.03 and (6) 0.04 M.

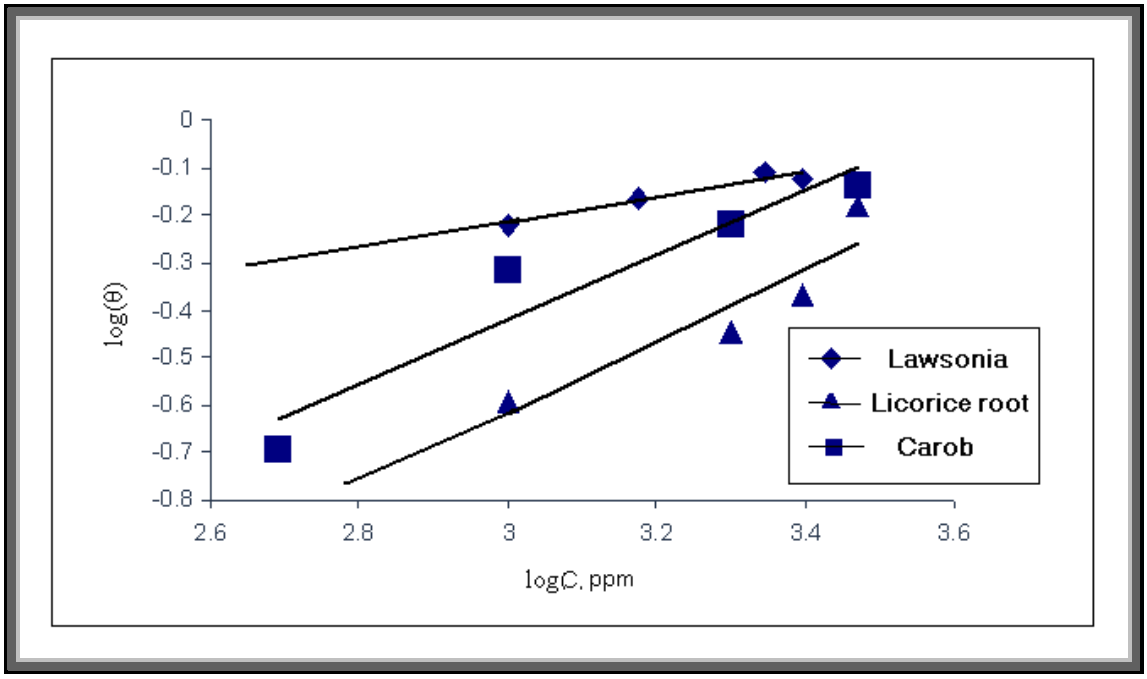

Fig.(3.29): The relation between log (θ) and log C, ppm for tin electrode in 0.6 M NaCl.

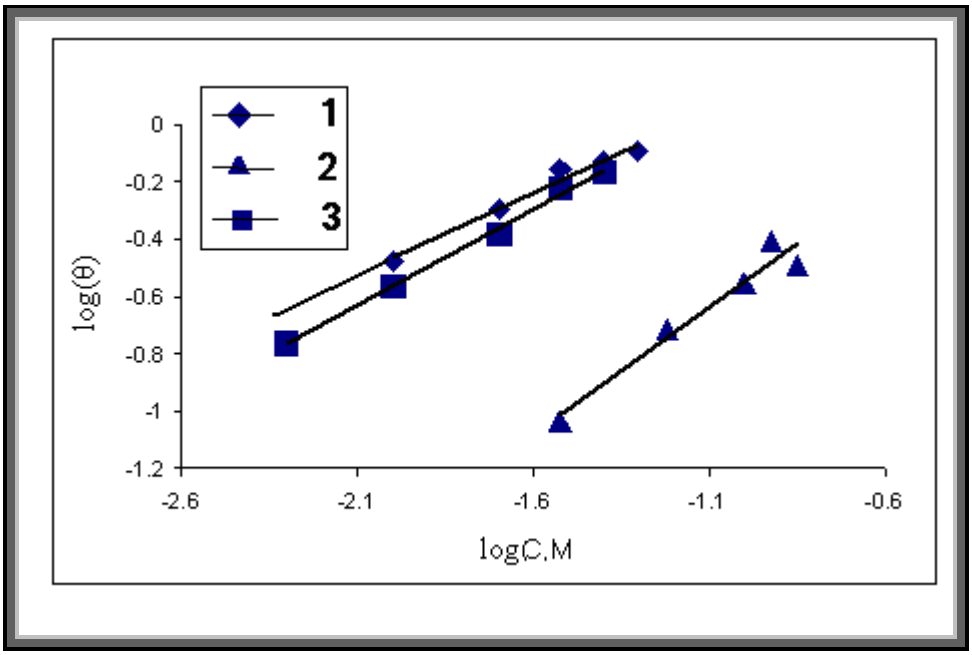

Fig.(3.30): The relation between log (θ) and log C, M for tin electrode in 0.6 M NaCl, where: 1) CrO_4^{2-} 2) WO_4^{2-} 3) HPO_4^{2-}.

Table (3.9): Corrosion parameters obtained from galvanostatic polarization measurements of tin electrode in 0.6 M NaCl solution containing different concentrations of lawsonia extract.

Inh. conc. (ppm)	**β_a mV. dec^{-1}**	**β_c mV. dec^{-1}**	**E_{corr} mV (SCE)**	**I_{corr} µA/cm^2**	**θ**	**%IE**
0	66.37	-1003.70	-886	17.130	-	-
1000	49.88	-711.69	-856	6.868	0.5991	59.91
1500	41.96	-501.06	-879	5.387	0.6855	68.55
2500	51.43	-481.16	-854	4.270	0.7507	75.07
3000	42.2	-410.95	-892	3.903	0.7722	77.22

Table (3.10): Corrosion parameters obtained from galvanostatic polarization measurements of tin electrode in 0.6 M NaCl solution containing different concentrations of licorice root extract.

Inh. conc. (ppm)	**β_a mV. dec^{-1}**	**β_c mV. dec^{-1}**	**E_{corr} mV (SCE)**	**I_{corr} µA/cm^2**	**θ**	**%IE**
0	66.37	-1003.70	-886	17.130	-	-
1000	55.23	-99.70	-886	13.260	0.2559	25.59
2000	61.87	-815.48	-866	10.994	0.3582	35.82
2500	79.22	-560.08	-835	9.798	0.4280	42.80
3000	0 61.9	-372.16	-896	5.793	0.6618	66.18

Table (3.11): Corrosion parameters obtained from galvanostatic polarization measurements of tin electrode in 0.6 M NaCl solution containing different concentrations of carob extract.

Inh. conc. (ppm)	**β_a mV. dec^{-1}**	**β_c mV. dec^{-1}**	**E_{corr} mV (SCE)**	**I_{corr} µA/cm^2**	**θ**	**%IE**
0	66.37	-1003.70	-886	17.130	-	-
500	58.52	-893.21	-871	13.640	0.2037	20.37
1000	43.20	-665.40	-900	8.863	0.4826	48.26
2000	50.41	-543.46	-903	6.787	0.6038	60.38
3000	52.84	-540.29	-889	4.541	0.7349	73.49

Table (3.12): Corrosion parameters obtained from galvanostatic polarization measurements of tin electrode in 0.6 M NaCl solution containing different concentrations of CrO_4^{2-} ions.

Inh. conc. (M)	**β_a mV. dec^{-1}**	**β_c mV. dec^{-1}**	**E_{corr} mV (SCE)**	**I_{corr} µA/cm^2**	**θ**	**%IE**
0	66.37	-1003.70	-886	17.130	-	-
0.01	114.85	-872.24	-834	11.406	0.3342	33.42
0.02	88.92	-610.82	-852	8.466	0.5058	50.58
0.03	68.64	-520.15	-888	5.125	0.7008	70.08
0.04	60.37	-440.18	-900	4.447	0.7404	74.04
0.05	59.34	-264.25	-904	3.308	0.8069	80.69

Table (3.13): Corrosion parameters obtained from galvanostatic polarization measurements of tin electrode in 0.6 M NaCl solution containing different concentrations of MoO_4^{2-} ions.

Inh. conc. (M)	**β_a mV. dec^{-1}**	**β_c mV. dec^{-1}**	**E_{corr} mV (SCE)**	**I_{corr} µA/cm^2**
0	66.37	-1003.70	-886	17.130
0.01	47.09	-544.56	-894	17.680
0.02	58.25	-496.23	-916	18.209
0.03	66.58	-328.88	-899	22.067
0.04	73.32	-350.48	-904	22.243
0.05	64.17	-245.77	-892	23.061

Table (3.14): Corrosion parameters obtained from galvanostatic polarization measurements of tin electrode in 0.6 M NaCl solution containing different concentrations of WO_4^{2-} ions.

Inh. conc. (M)	**β_a mV. dec^{-1}**	**β_c mV. dec^{-1}**	**E_{corr} mV (SCE)**	**I_{corr} µA/cm^2**	**θ**	**%IE**
0	66.37	-1003.70	-886	17.130	-	-
0.03	53.68	-568.71	-910	15.556	0.0919	9.19
0.06	48.95	-564.64	-915	13.802	0.1943	19.43
0.1	44.66	-431.21	-912	12.319	0.2809	28.09
0.12	51.16	-437.16	-883	10.383	0.3939	39.39
0.14	47.22	-345.23	-921	11.546	0.3260	32.60

Table (3.15): Corrosion parameters obtained from galvanostatic polarization measurements of tin electrode in 0.6 M NaCl solution containing different concentrations of HPO_4^{2-} ions.

Inh. conc. (M)	**β_a mV. dec^{-1}**	**β_c mV. dec^{-1}**	**E_{corr} mV (SCE)**	**I_{corr} µA/cm^2**	**θ**	**%IE**
0	66.37	-1003.70	-886	17.130	-	-
0.005	57.69	-816.80	-876	14.179	0.1723	17.23
0.01	65.58	-517.52	-872	12.468	0.2722	27.22
0.02	66.81	-374.84	-843	9.991	0.4158	41.68
0.03	71.49	-327.49	-806	6.944	0.5946	59.46
0.04	54.10	-208.43	-841	5.395	0.6851	68.51

Table (3.16): Equilibrium constant and the adsorption free energy of the inhibitors adsorbed on the surface of tin electrode in 0.6 M NaCl.

Inhibitor type	**K**	**ΔG^{o}_{ads} Cal. mol^{-1}**
Lawsonia	0.093	-426.4
Licorice root	0.030	-133.5
Carob	0.056	-294.4
CrO_4^{2-}	4.600	-1432.3
WO_4^{2-}	2.200	-1245.3
HPO_4^{2-}	6.000	-1503.2

Section (3)

Initiation and Inhibition of Pitting Corrosion

3.3.1 Pitting corrosion of tin in $NaHCO_3$ solutions and its inhibition.

3.3.1.1 Initiation pitting corrosion of tin in $NaHCO_3$ solutions.

Pitting corrosion of tin like other metals or alloys occurs when passivity breakdown takes place at local points on the surface exposing them to the corrosive environment and at those points the anodic dissolution proceeds whilst the most part of the surface remains passive.

Two basic conditions must be fulfilled for the initiation and propagation of pitting corrosion. Firstly, the major part is that the metal surface should be covered with an electronically conducting passivating inhibiting film or which the cathodic partial reaction takes place.

This film can be formed naturally or be produced through alloying with an appropriate metal or by oxidizing agents with redox potentials equal to, or higher than, the corresponding flade potential and or by anodic protection. Secondly, the medium should contain an aggressive agent. Chloride ions are the most dangerous pitting agent and for this reason pitting corrosion is some times referred to as "chloride corrosion". The other halogen ions also cause pitting corrosion but to a less extent. Similarly under certain condition perchlorate [123] sulphates [124] may cause localized corrosion.

3.3.1.2 Effect of NaCl concentration on the pitting corrosion of tin electrode in $NaHCO_3$ solutions.

In this part the effect of addition different concentrations of NaCl on the pitting corrosion of tin electrode in 0.1 M $NaHCO_3$ solution was examined by potentiodynamic anodic polarization technique.

Fig. (3.31) shows the potentiodynamic anodic polarization curves of tin electrode in 0.1 M $NaHCO_3$ solution using different concentrations of NaCl at scan rate 1mV/s. The slow scan rate permits that the pitting initiation occurs at less positive potential [125]. It is clear from the results that in the concentration range of NaCl studied the metal does not exhibit an active-transition. However, on increasing the concentration of Cl^- ions, there is a sudden and marked increase of current density at a definite potential indicating the passivity breakdown and initiation of pitting corrosion [126]. The potential at which the sudden rise takes place is defined as the pitting potential (E_{pit}).The higher concentration of Cl^- ions; the higher is the shift of pitting potential towards the active direction. The breakdown of passivity could be attributed to the adsorption of chloride ions on the passive film formed on the tin surface, which create an electrostatic field across film/solution interface [127-128]. Thus, when the electrostatic field reaches a certain value, the adsorbed anions begin to penetrate into the passive film and the pitting corrosion is initiated.

The dependence of E_{pit} with the concentration of Cl^- ions is shown in Fig. (3.32) the relation gives straight line curve in the following form [129]:

$$E_{pit} = a_1 - b_1 \log C_{Cl^-} \qquad (3.14)$$

where a_1 and b_1 are constants depending on both the nature and type of the aggressive anion and of the electrode. As the concentration of chloride ions increases the pitting potential is shifted to more negative direction

indicating the destruction of the passive film and initiation of pitting corrosion.

The differential between pit initiation and pit propagation is well explained by Aziz and Godard [130]. A pit can be started by artificial stimulation at otherwise normal sites on the metal surface. Yet continue to propagate if given the right environmental conditions. This concept has been widely used to explain pitting corrosion phenomena.

Hoars et al. [131] related pit initiation on a supposed oxide film, followed by their penetration through the film (without exchange) under the influence of an electrostatic field across the film solution interface. When the latter field reaches a certain critical value, corresponding to the pitting potential, pitting occurs, and the oxide film is presumably undetermined either by vacancy condensation at the metal interface, or it releases cations rapidly at the electrolyte interface so that in either cases pitting proceeds. The introduction period for pitting to occur is related to the time required for supposed penetration of the ions through the oxide film. Regarding this mechanism Leckie and Uhlig [132]argued that, if this is correct, either anion of large molecular size than the halogen ions e.g. SO_4^{2-}, ClO_4^-, NO_3^- and OH^-, which are practically having no pitting tendency, can also penetrate the passive oxide film causing the formation of pit.

The latter author [132] proposed another model based on the visible competitive adsorption of the aggressive ions with oxygen for adsorption sites on the metal surface. This model is based on the assumption that adsorbed oxygen rather than oxide is the cause of passive formation. Oxygen has normally higher affinity than Cl^- ions for adsorption sites on the metal surface, but as the potential of the working electrode is shifted

into the passive direction, higher Cl^- ions move into the double layer when the concentration of the latter reaches a certain definite value, corresponding to the pitting potential, it succeed at favored sites in destroying passivity by displacing adsorbed O_2 ions. This introduction time for pitting is attributed here to the slow process of competitive adsorption. It is of interest to mention that similar view was also, reported by Koltrykin [133], Rosenfeld [134] and Schwenk et al [135].

It contrast to the model of competitive adsorption, Foroulis and Thubriker [136] based their argument on the findings that, the critical pitting potential of the polarized depends on the thickness of oxide film at the metal surface. They concluded that, if competitive adsorption at the metal surface the controlling mechanism, then the thickness of any overlying oxide would have no influence on the critical potential at which the Cl^- ions displace the adsorbed oxygen on the metal bare.

Abd El-Haleem [137] assumed that the initiation of pitting on Zn-Ti-Cu alloy involves, as a rate controlling step, the adsorption of chloride ions on a layer of mixed oxide/hydroxide of Zn, Ti and/or Cu followed by the formation of the corresponding chloro-metal oxide or hydroxide complexes. The deadly soluble of these complexes can go into solution, most probably the Zn complexes as soluble Zn^{2+}. This result in pit initiation with continues anodic dissolution of Zn^{2+} at the point of attack. This latter model was confirmed by the use of the electron microscope analyzer of performed pit.

3.3.1.3 Inhibition of pitting corrosion of tin electrode in 0.1 M $NaHCO_3$ + 0.1 M NaCl solution.

In the present chapter, trials are made to inhibit the pitting corrosion of tin by some naturally occurring substances such as the extracts of lawsonia, licorice root and carob. Also some inorganic compounds such as the sodium salts of CrO_4^{2-}, MoO_4^{2-}, WO_4^{2-} and HPO_4^{2-} ions are used to inhibit the pitting corrosion of tin.

Figs. (3.33-3.35) represent the effect of addition of increasing concentration of naturally occurring substances e.g. lawsonia, licorice root and carob extracts, respectively, on the potentiodynamic anodic polarization curves of tin electrode in 0.1 M $NaHCO_3$ + 0.1 M NaCl solution at scan rate 1 mV/sec.

Also, Figs. (3.37-3.40) represent the effect of addition of increasing concentrations of some inorganic compounds such as sodium salts of CrO_4^{2-}, MoO_4^{2-}, WO_4^{2-} and HPO_4^{2-} ions, respectively, on the potentiodynamic anodic polarization curves of tin electrode in 0.1 M $NaHCO_3$ + 0.1 M NaCl solution at scan rate 1 mV/sec.

Inspection of the curves of these figures reveal that the presence of an increased concentration of these compounds causes a marked shift of the pitting corrosion potential into noble (positive) direction. This shift indicates an increased resistance to pitting attack.

The dependence of pitting corrosion potential (E_{pit}) of the tin electrode on the concentrations of the plants extracted compounds can be seen from Fig. (3.36) which represents the relationship between the pitting potential (E_{pit}) versus the logarithm of concentrations of the plants extracted compounds.

Fig. (3.41) represents the same relation but in presence of the sodium salts of inorganic compounds.

From the curves of Fig. (3.36) it is obvious that, the presence of increasing concentrations of the plants extracted compounds causes the shift of the pitting potential into the noble direction in accordance with the following equation:

$$E_{pit} = a_1 + b_1 \log C_{inh.} \quad (3.15)$$

where a and b are constants that depend on the type of both the inhibitor and aggressive anion as well as on the metal used. But in Fig. (3.41) broken lines were obtained. The pitting potential depending on the concentration of inorganic compounds used. At low inhibitor concentrations, the E_{pit} is shifted slightly to more positive direction, and at higher concentration of additives the E_{pit} is shifted rapidly to more positive direction satisfy the equation (3.15).

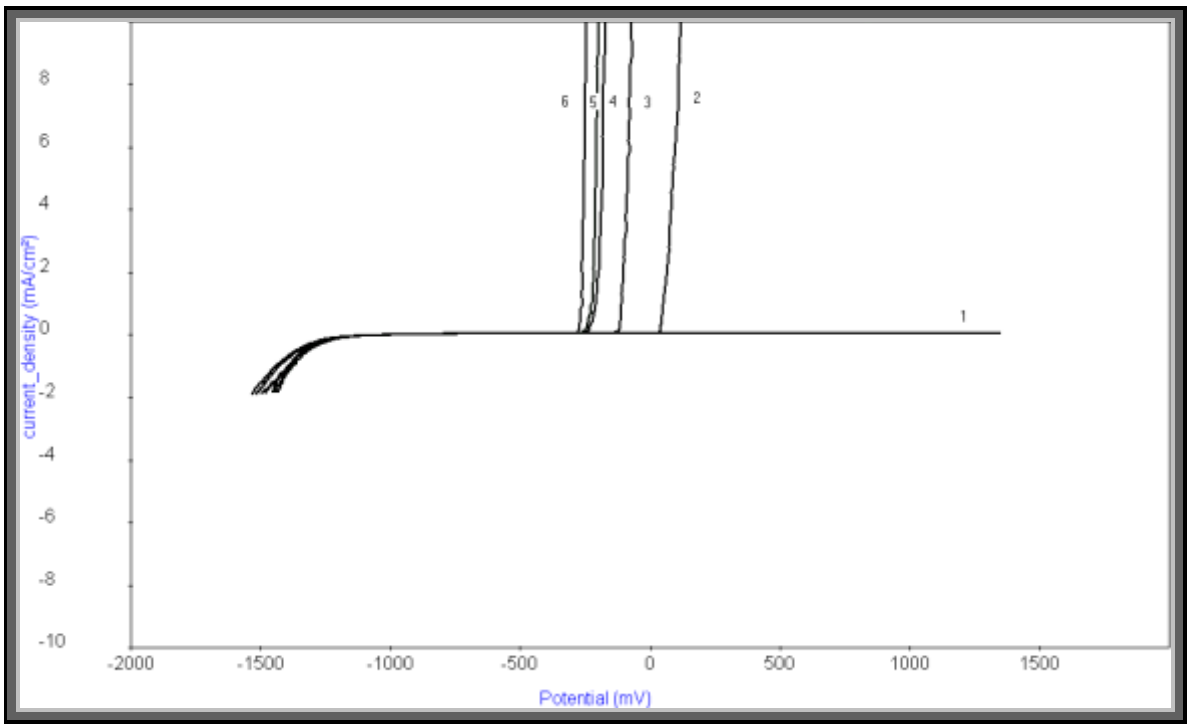

Fig.(3.31): Polarization curves for tin electrode in 0.1 M $NaHCO_3$ and different concentrations of NaCl at scan rate 1 mV/sec. (1) 0, (2) 0.1, (3) 0.3, (4) 0.5, (5) 0.6 and (6) 1 M.

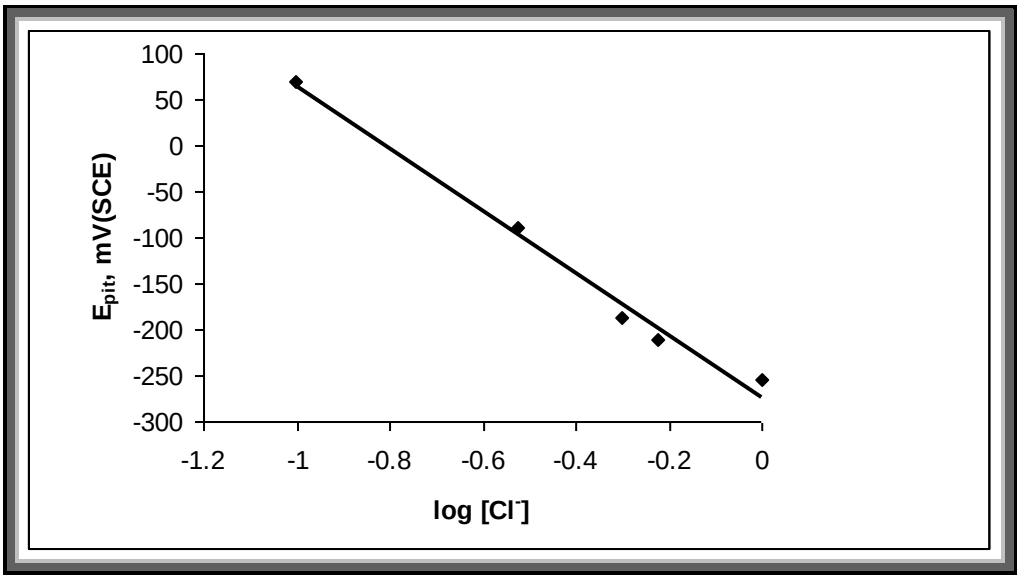

Fig.(3.32): The relation between the pitting potential (E_{pit}) and log [Cl^-].

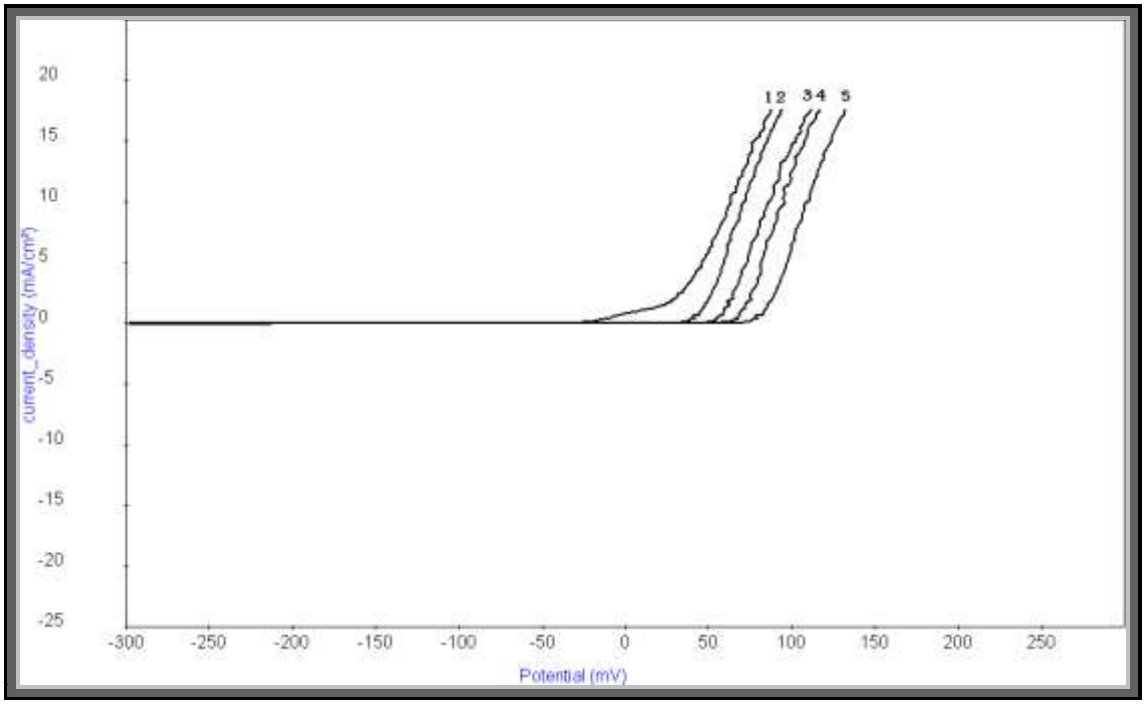

Fig.(3.33): Potentiodynamic anodic polarization curves for tin electrode in 0.1 M $NaHCO_3$ + 0.1 M NaCl and different concentrations of lawsonia extract at scan rate 1 mV/sec. (1) 0, (2) 500, (3) 1000, (4) 1500 and (5) 1600 ppm.

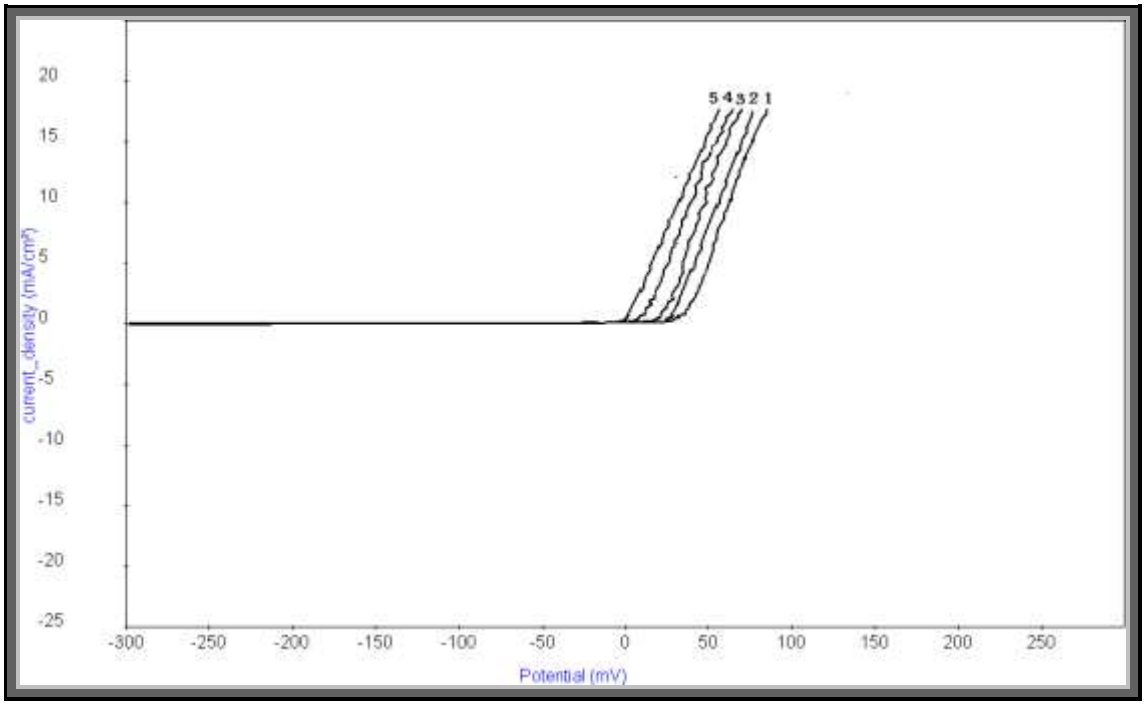

Fig.(3.34): Potentiodynamic anodic polarization curves for tin electrode in 0.1 M $NaHCO_3$ + 0.1 M NaCl and different concentrations of licorice root extract at scan rate 1 mV/sec. (1) 0, (2) 500, (3) 1000, (4) 1500 and (5) 2500 ppm.

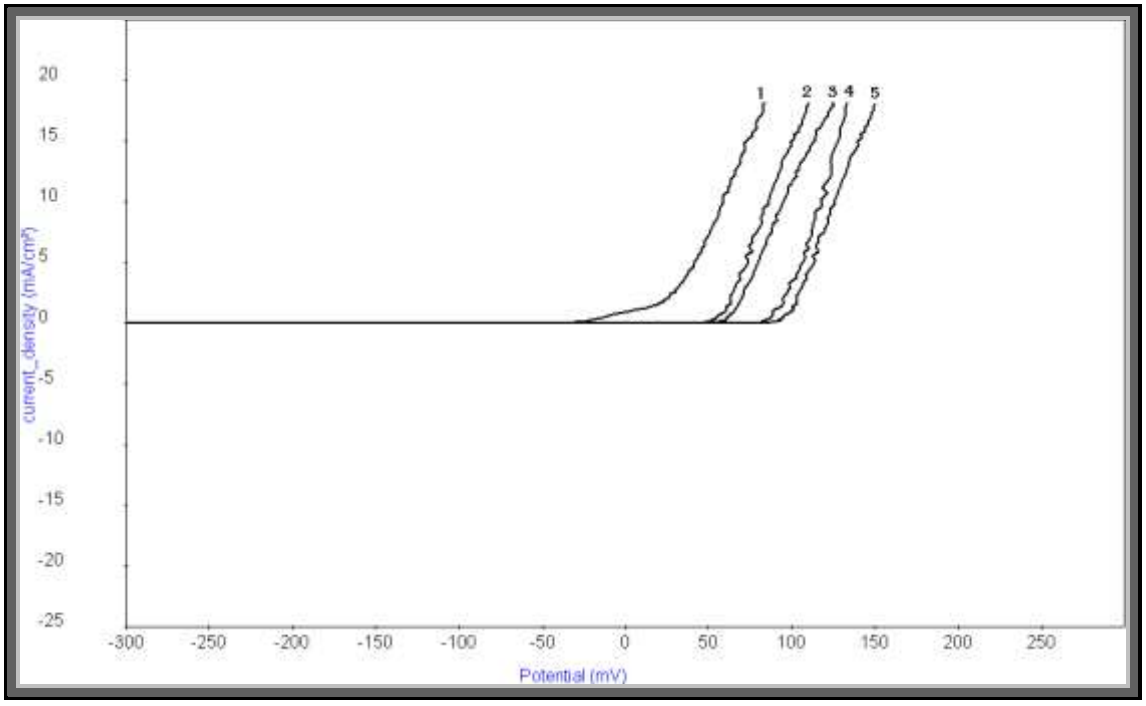

Fig.(3.35): Potentiodynamic anodic polarization curves for tin electrode in 0.1 M $NaHCO_3$ + 0.1 M NaCl and different concentrations of carob extract at scan rate 1 mV/sec. (1) 0, (2) 500, (3) 1000, (4) 2000 and (5) 3000 ppm.

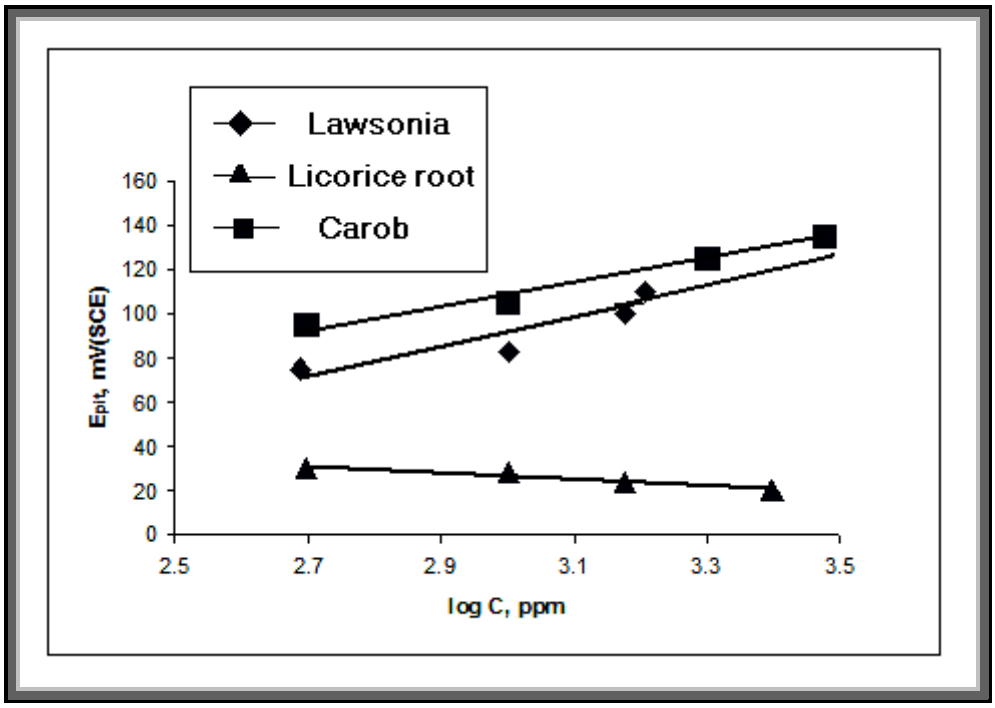

Fig.(3.36): The relation between the pitting potential of tin and logarithm of the concentrations of the plants extracts.

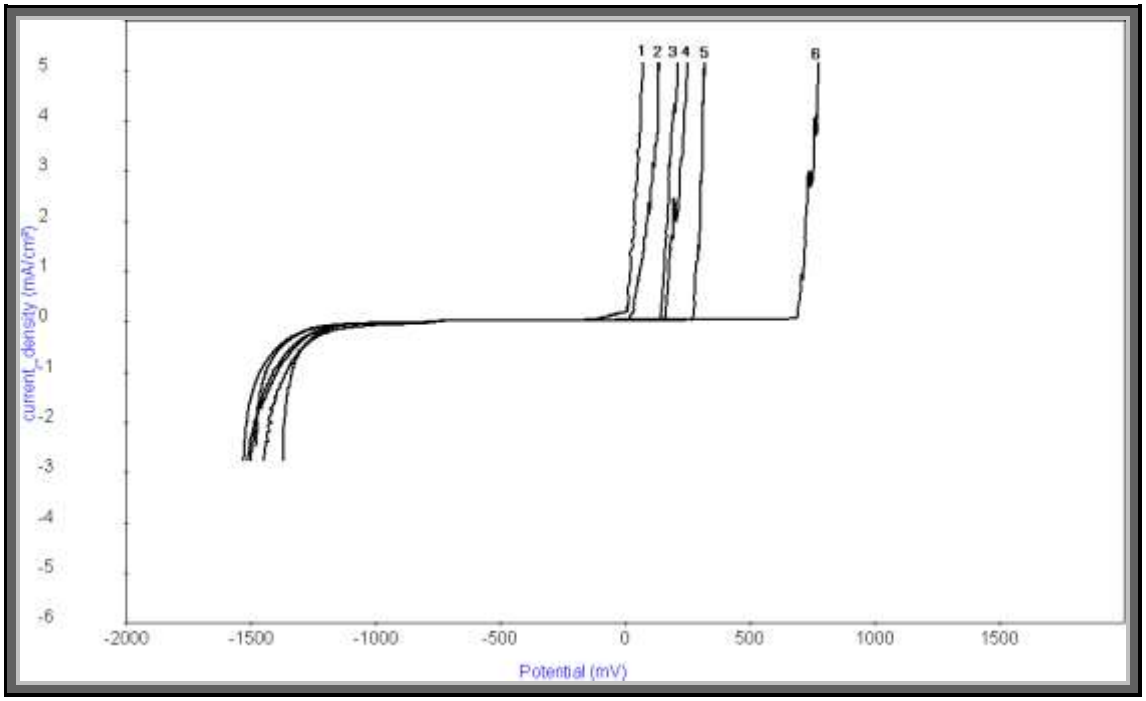

Fig.(3.37): Potentiodynamic anodic polarization curves for tin electrode in 0.1 M $NaHCO_3$ + 0.1 M NaCl and different concentrations of CrO_4^{2-} ions at scan rate 1 mV/sec. (1) 0, (2) 0.004, (3) 0.006, (4) 0.008, (5) 0.01 and (6) 0.012 M.

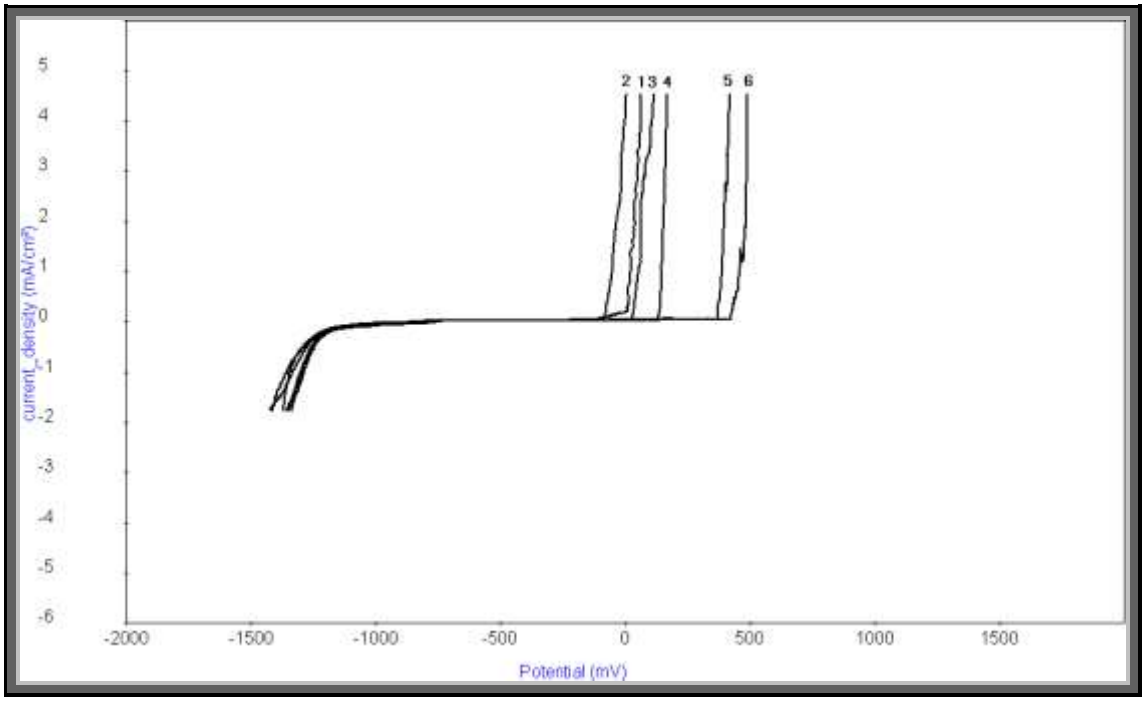

Fig.(3.38): Potentiodynamic anodic polarization curves for tin electrode in 0.1 M $NaHCO_3$ + 0.1 M NaCl and different concentrations of MoO_4^{2-} ions at scan rate 1 mV/sec. (1) 0, (2) 0.01, (3) 0.02, (4) 0.03, (5) 0.04 and (6) 0.05 M.

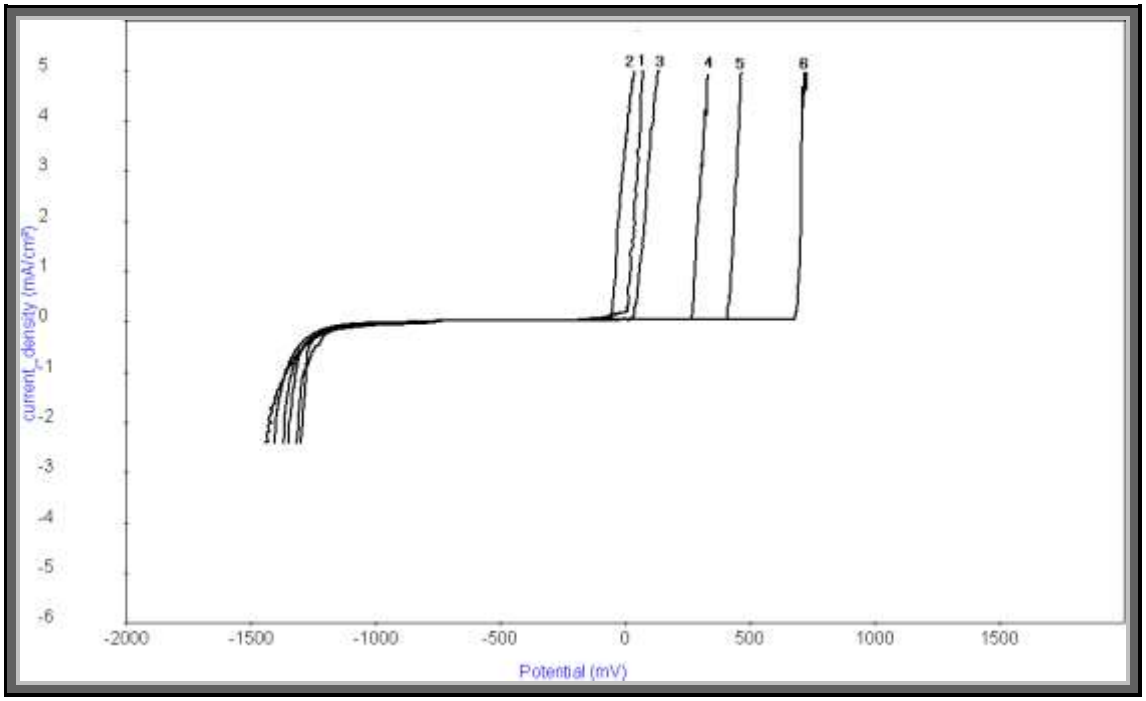

Fig.(3.39): Potentiodynamic anodic polarization curves for tin electrode in 0.1 M $NaHCO_3$ + 0.1 M NaCl and different concentrations of WO_4^{2-} ions at scan rate 1 mV/sec. (1) 0, (2) 0.01, (3) 0.02, (4) 0.025, (5) 0.035 and (6) 0.04 M.

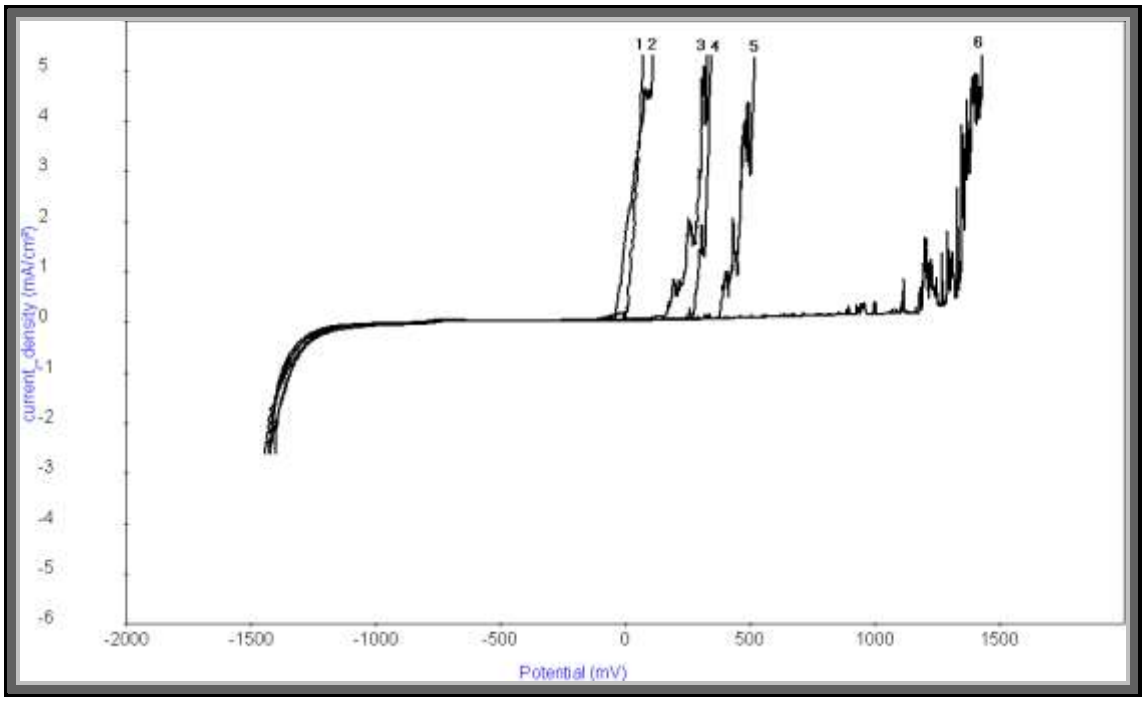

Fig.(3.40): Potentiodynamic anodic polarization curves for tin electrode in 0.1 M $NaHCO_3$ + 0.1 M NaCl and different concentrations of HPO_4^{2-} ions at scan rate 1 mV/sec. (1) 0, (2) 0.01, (3) 0.04, (4) 0.05, (5) 0.055 and (6) 0.06 M.

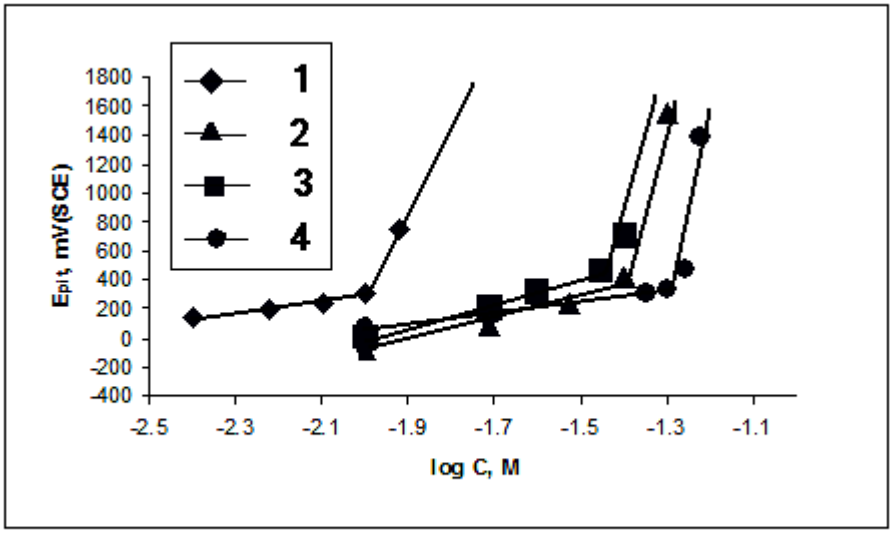

Fig.(3.41): The relation between the pitting potential of tin and logarithm of the concentrations of inorganic compounds, where: 1) CrO_4^{2-} 2) MoO_4^{2-} 3) WO_4^{2-} 4) HPO_4^{2-}.

3.3.2 Inhibition of the pitting corrosion of tin electrode in NaCl solutions.

3.3.2.1 Effect of NaCl concentration on pitting corrosion of tin electrode in distilled water.

In this part the effect of addition different concentrations of NaCl on the pitting corrosion of tin electrode in distilled water was examined by potentiodynamic anodic polarization technique.

Fig. (3.42) shows the potentiodynamic anodic polarization curves of tin electrode in distilled water using different concentrations of NaCl at scan rate 1mV/s. The slow scan rate permits that the pitting initiation occurs at less positive potential [116]. It is clear from the results that the higher concentration of Cl^- ions, the higher is the shift of pitting potential towards the active direction.

The dependence of E_{pit} with the concentration of Cl^- ions is shown in Fig. (3.43), the relation gives straight line curve according to equation (3.14). This indicates that, as the concentration of Cl^- ions increases the pitting potential is shifted to more negative direction i.e. accelerate the pitting corrosion.

3.3.2.2 Effect of inhibitors on the pitting corrosion of tin electrode in 0.6 M NaCl solution.

Figs. (3.44-3.46) represent the effect of addition of increasing concentration of natural occurring substances e.g. lawsonia, licorice root and carob extracts, respectively, on the potentiodynamic anodic polarization curves of tin electrode in 0.6 M NaCl solution at scan rate 1 mV/sec.

Figs. (3.48-3.51) represents the effect of addition of increasing concentrations of some inorganic compounds such as sodium salts of CrO_4^{2-}, MoO_4^{2-}, WO_4^{2-} and HPO_4^{2-} ions, respectively, on the potentiodynamic anodic polarization curves of tin electrode in 0.6 M NaCl solution at scan rate 1 mV/sec.

Fig. (3.47) represents the variation of the pitting potential with the logarithm of concentration of the plants extracted compounds for tin.

Fig. (3.52) represents the variation of the pitting potential with the logarithm of concentration of CrO_4^{2-}, MoO_4^{2-}, WO_4^{2-} and HPO_4^{2-} ions, respectively, for tin.

Inspection of the curves in Figs. (3.47 and 3.52), it is clear that, the increasing concentration of additive compounds (plants extracts and inorganic compounds) causes the shift of the pitting potential to more positive direction satisfying the equation (3.15). This indicates that the inhibition of pitting corrosion of tin in 0.6 M NaCl.

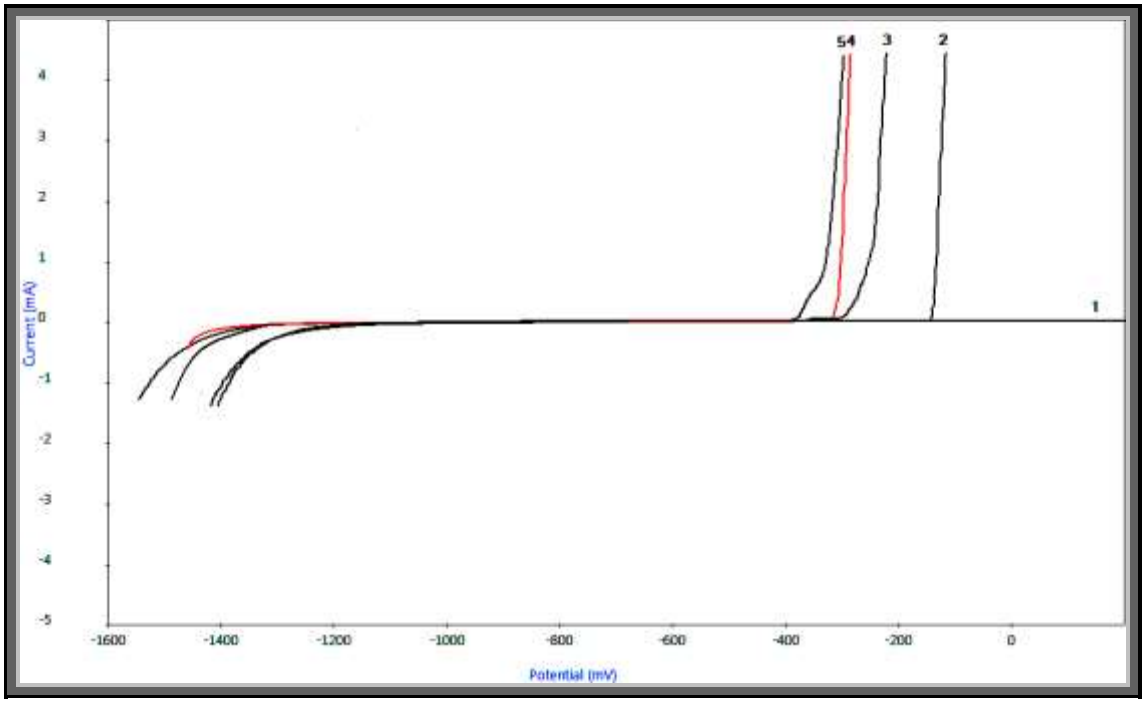

Fig.(3.42): Polarization curves for tin electrode in distilled water and different concentrations of NaCl at scan rate 1 mV/sec. (1) 0, (2) 0.2, (3) 0.3, (4) 0.4 and (5) 0.6 M.

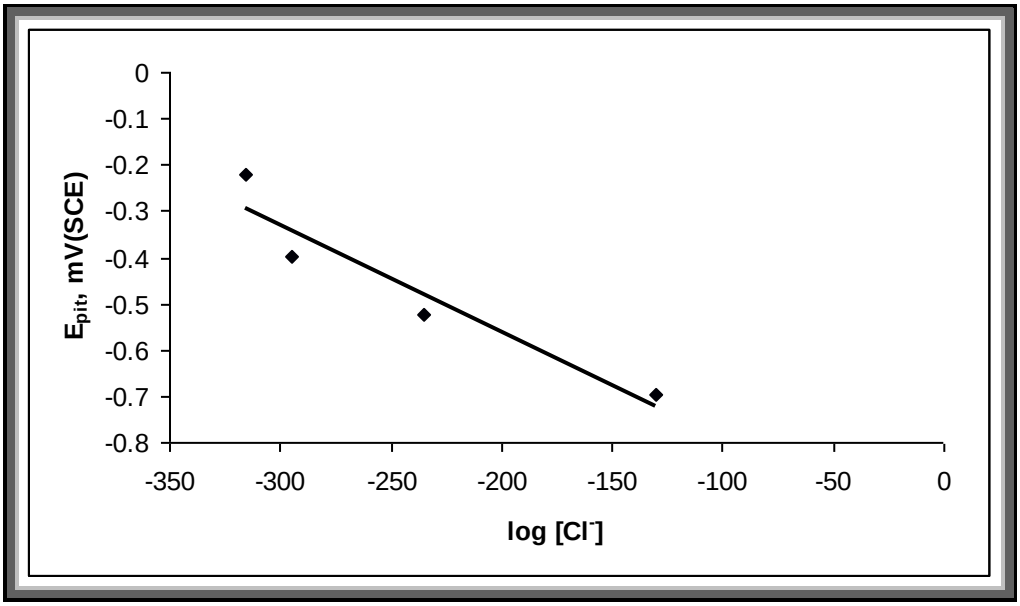

Fig.(3.43): The relation between the pitting potential (E_{pit}) and log [Cl^-].

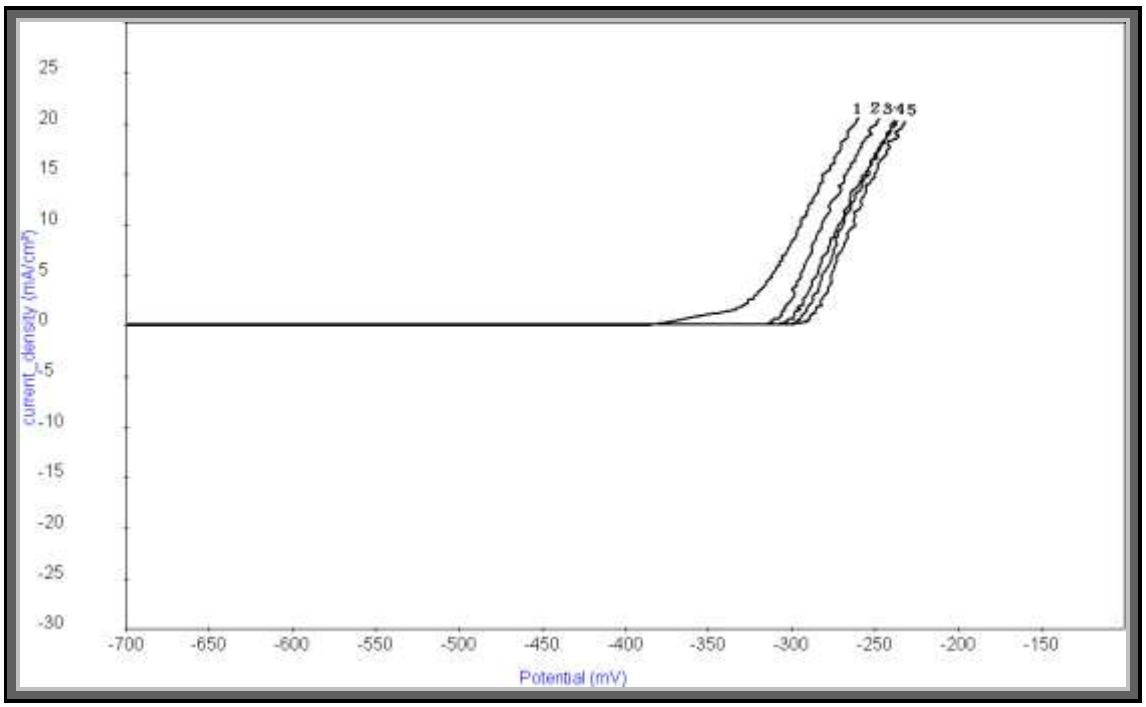

Fig.(3.44): Potentiodynamic anodic polarization curves for tin electrode in 0.6 M NaCl and different concentrations of lawsonia extract at scan rate 1 mV/sec. (1) 0, (2) 1000, (3) 1500, (4) 2500 and (5) 3000 ppm.

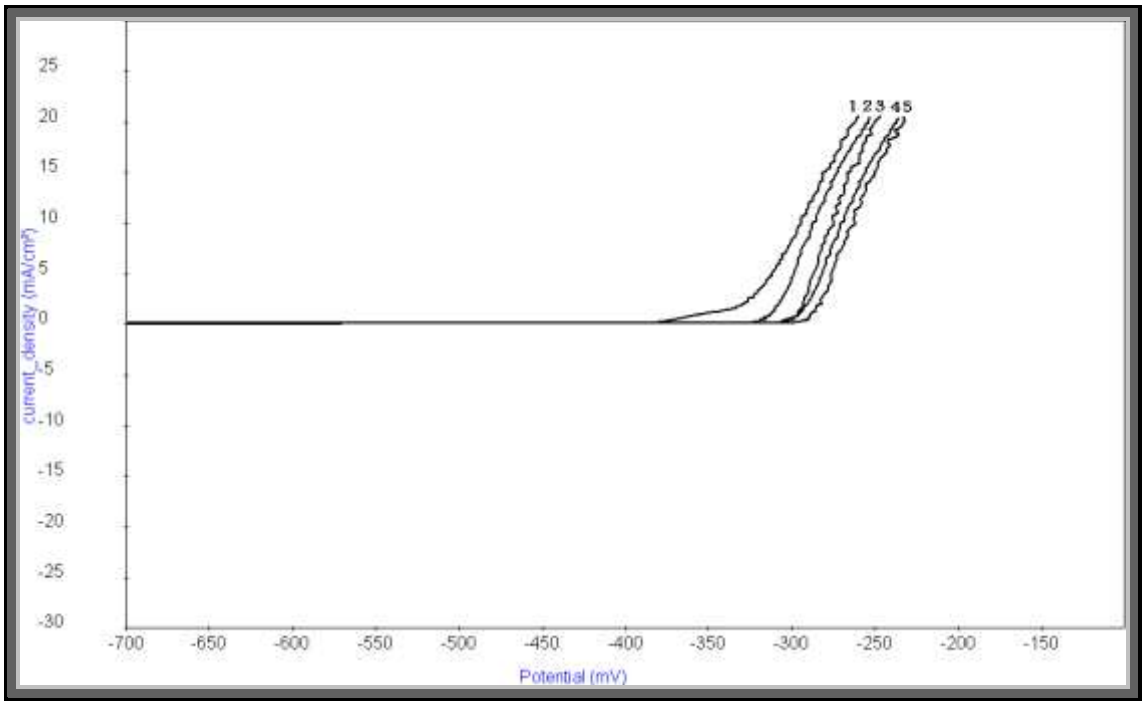

Fig.(3.45): Potentiodynamic anodic polarization curves for tin electrode in 0.6 M NaCl and different concentrations of licorice root extract at scan rate 1 mV/sec. (1) 0, (2) 1000, (3) 2000, (4) 2500 and (5) 3000 ppm.

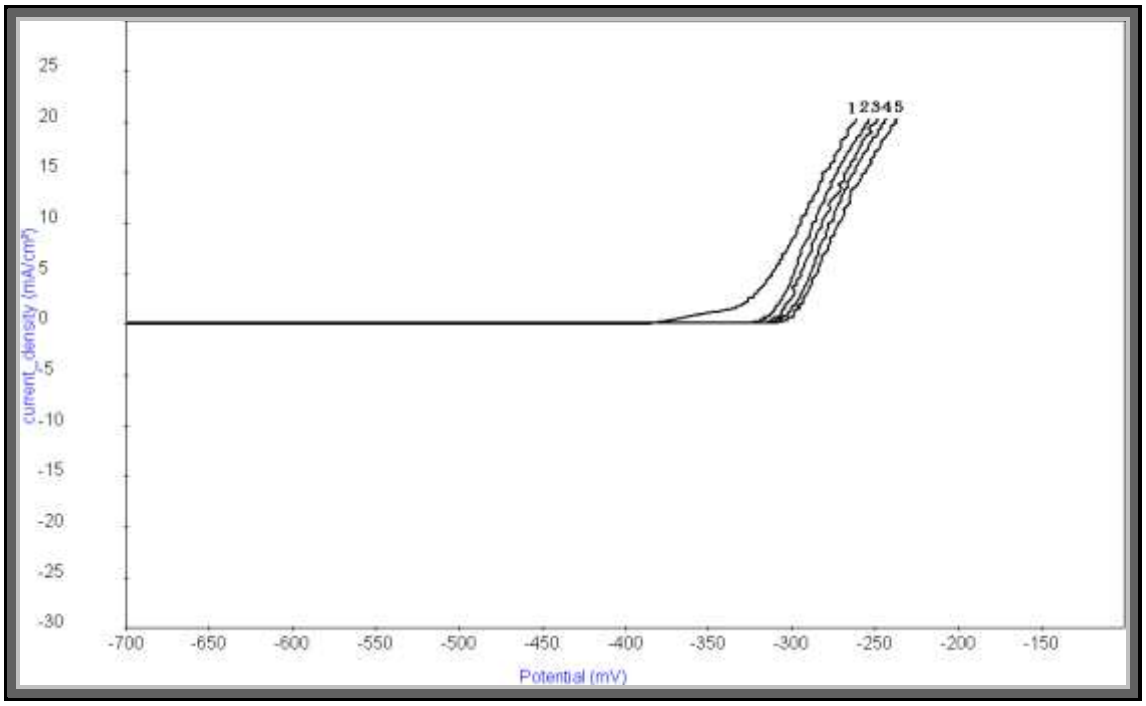

Fig.(3.46): Potentiodynamic anodic polarization curves for tin electrode in 0.6 M NaCl and different concentrations of carob extract at scan rate 1 mV/sec. (1) 0, (2) 500, (3) 1000, (4) 2000 and (5) 3000 ppm.

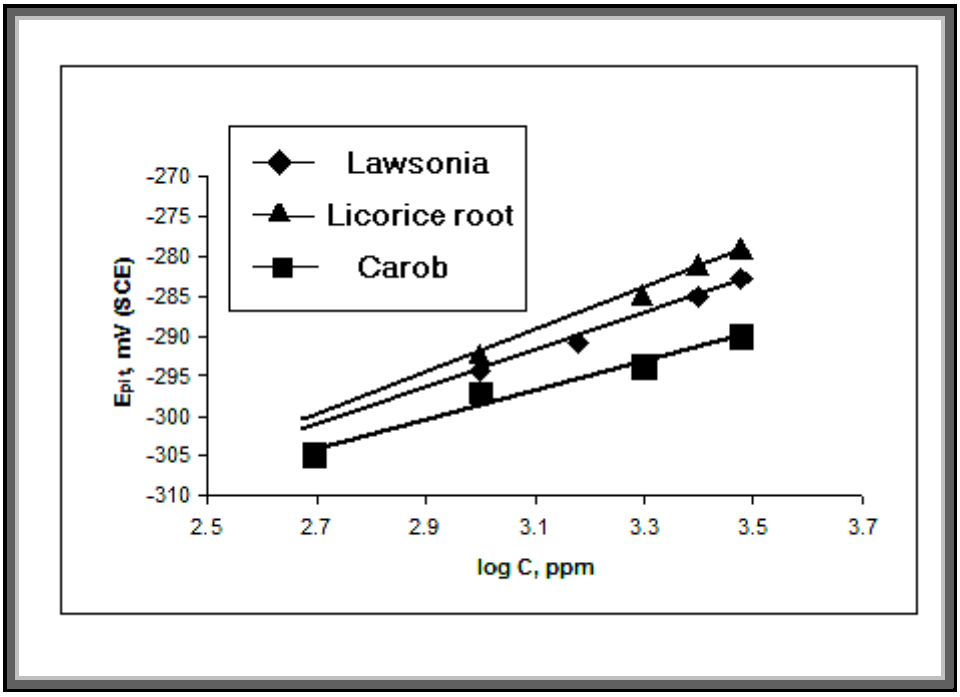

Fig.(3.47): The relation between the pitting potential (E_{pit}) and log C, ppm.

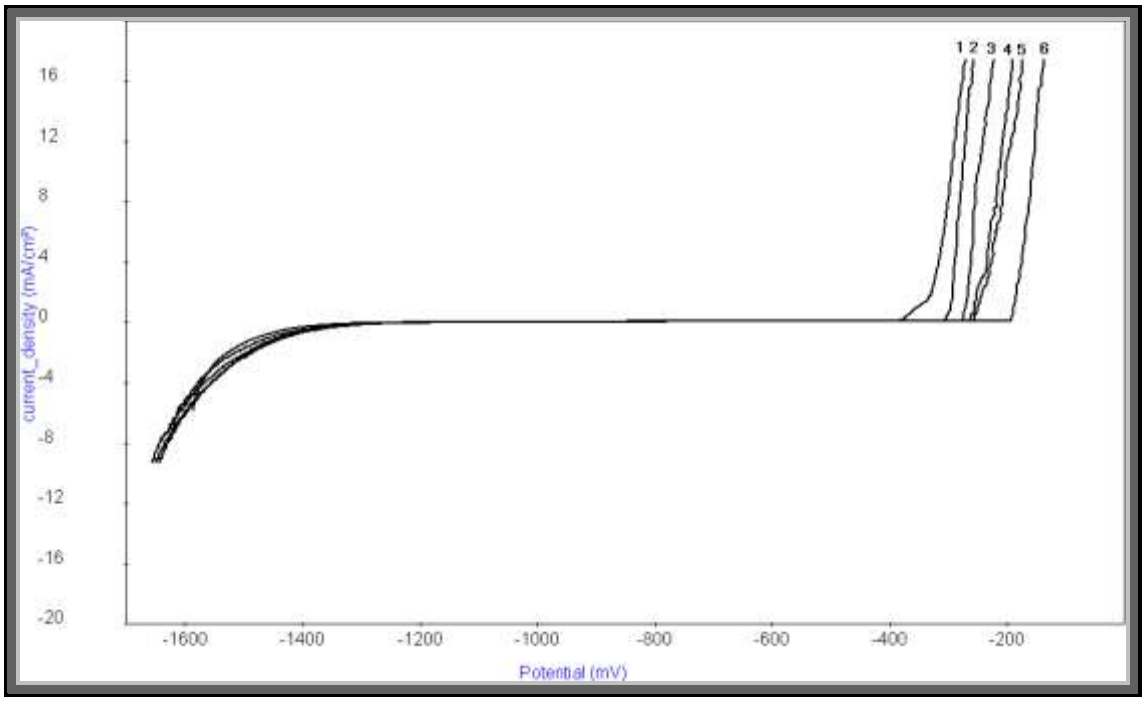

Fig.(3.48): Potentiodynamic anodic polarization curves for tin electrode in 0.6 M NaCl and different concentrations of CrO_4^{2-} ions at scan rate 1 mV/sec. (1) 0, (2) 0.01, (3) 0.02, (4) 0.03, (5) 0.04 and (6) 0.05 M.

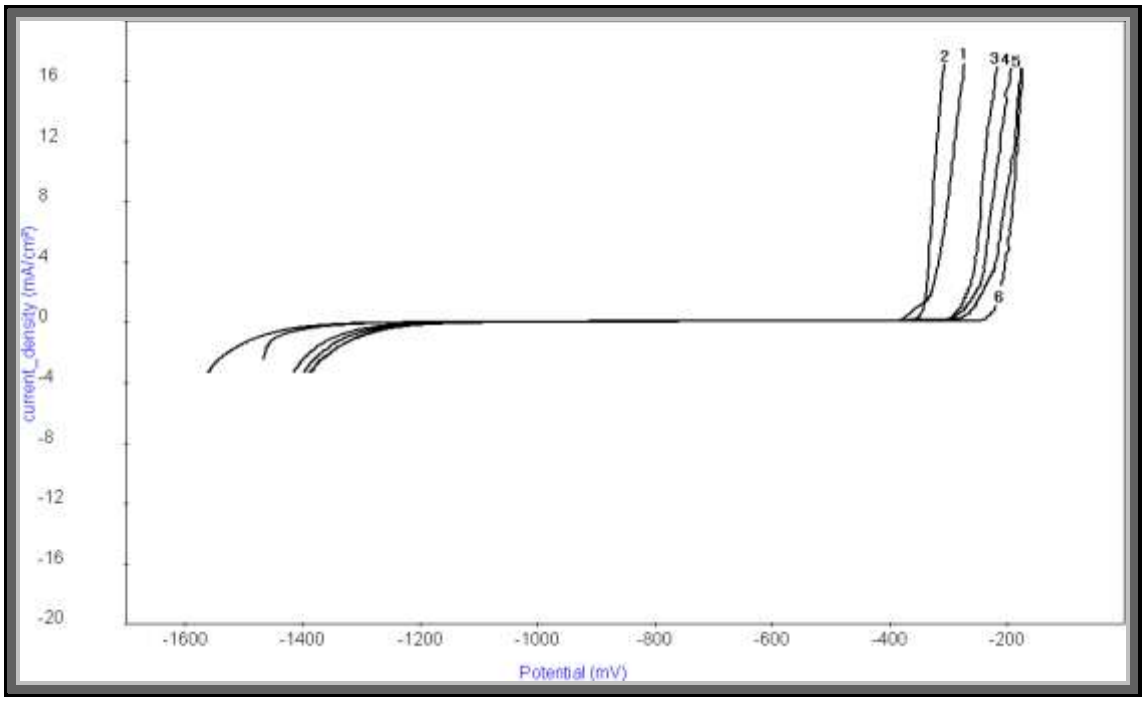

Fig.(3.49): Potentiodynamic anodic polarization curves for tin electrode in 0.6 M NaCl and different concentrations of MoO_4^{2-} ions at scan rate 1 mV/sec. (1) 0, (2) 0.01, (3) 0.02, (4) 0.03, (5) 0.04, (6) 0.05 M.

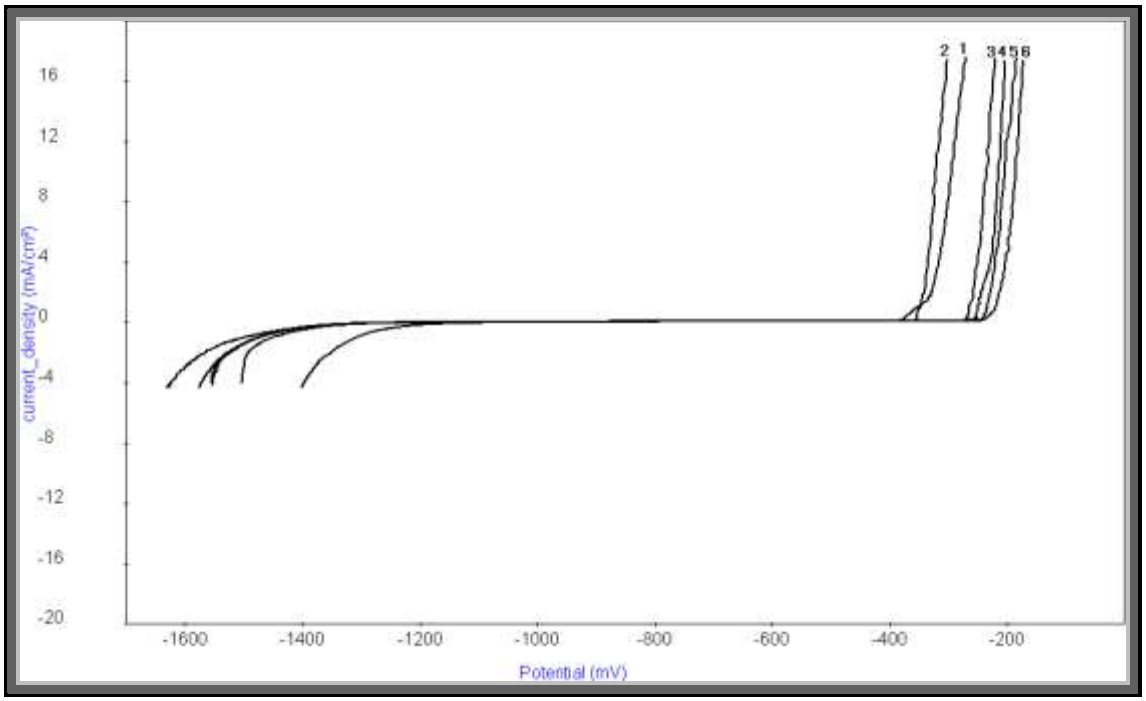

Fig.(3.50): Potentiodynamic anodic polarization curves for tin electrode in 0.6 M NaCl and different concentrations of WO_4^{2-} ions at scan rate 1 mV/sec. (1) 0, (2) 0.03, (3) 0.06, (4) 0.1, (5) 0.12 and (6) 0.14 M.

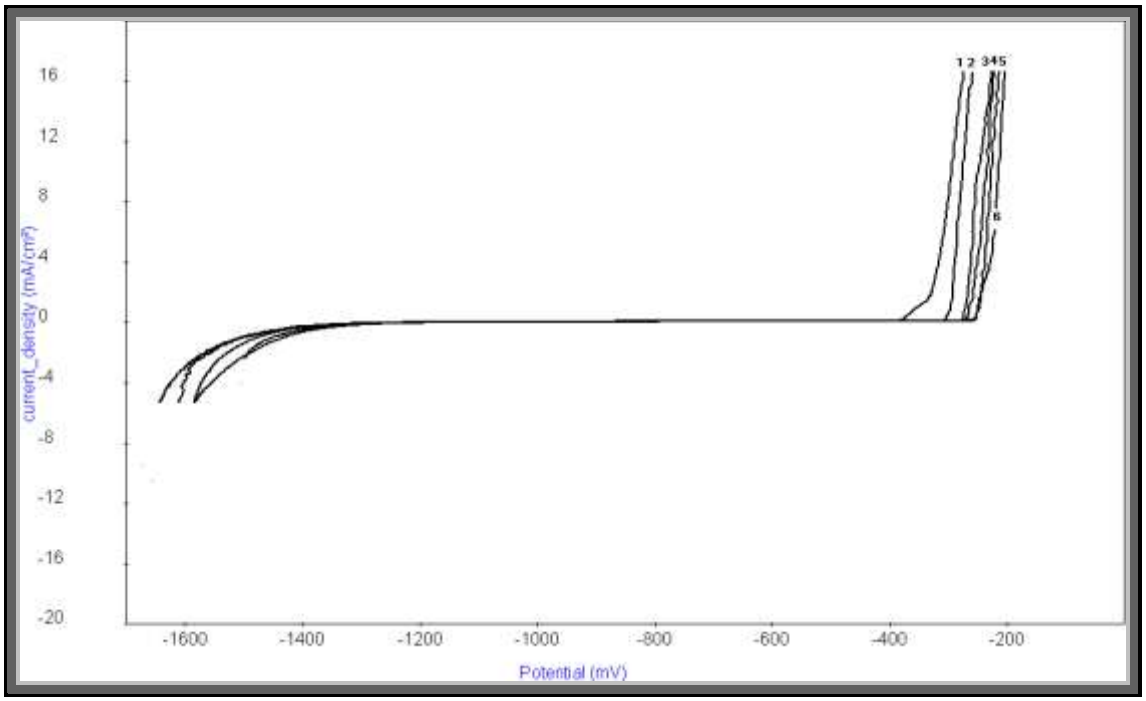

Fig.(3.51): Potentiodynamic anodic polarization curves for tin electrode in 0.6 M NaCl and different concentrations of HPO_4^{2-} ions at scan rate 1 mV/sec. (1) 0, (2) 0.005, (3) 0.01, (4) 0.02, (5) 0.03 and (6) 0.04 M.

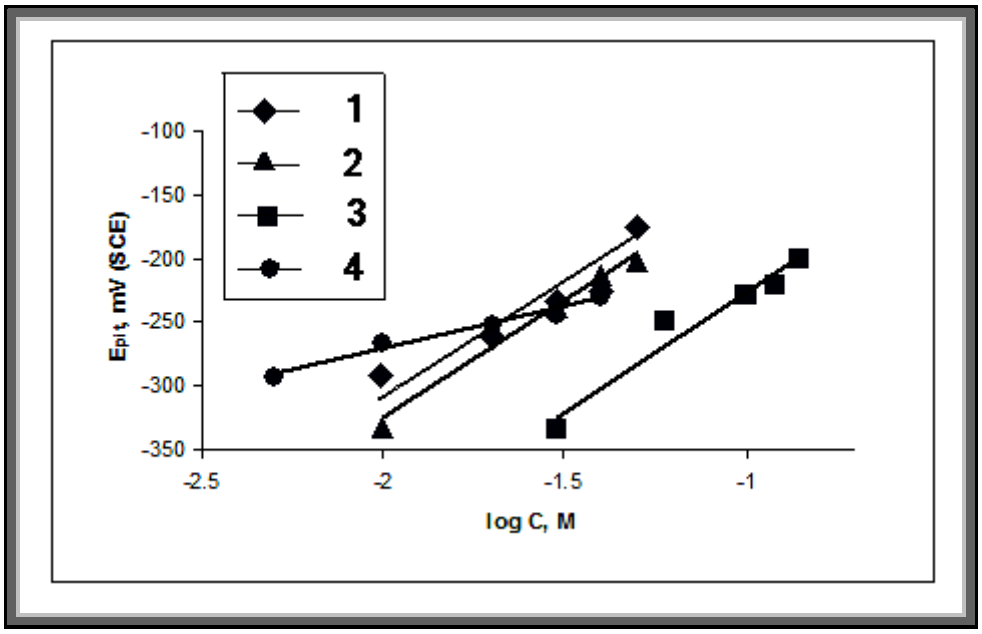

Fig.(3.52): The relation between the pitting potential (E_{pit}) and log C, M , where: 1) CrO_4^{2-} 2) MoO_4^{2-} 3) WO_4^{2-} 4) HPO_4^{2-}.

Section (4)

Mechanism of Inhibition

The inhibition of corrosion of tin electrode in 0.1 M $NaHCO_3$ and in 0.6 M NaCl solutions and pitting corrosion in 0.1 M $NaHCO_3$ + 0.1 M NaCl and in 0.6 M NaCl solutions by some naturally occurring substance e.g. lawsonia, licorice root and carob and inorganic compounds e.g. the sodium salts of CrO_4^{2-}, MoO_4^{2-}, WO_4^{2-} and HPO_4^{2-} ions were studied. Galvanostatic polarization and potentiodynamic anodic polarization techniques were used in this study.

The inhibition efficiency was found to depend on both the concentration and the nature of the inhibitors. As the concentration of the inhibitors increase the observed corrosion parameters led to:

i- Decrease of corrosion current density.

ii- Increase of inhibition efficiency.

iii- Increase of surface coverage.

iv- Shift of pitting potential to positive direction.

It is generally believed that the adsorption of the inhibitor at the metal/solution interface is the first step in the mechanism of inhibitor action in aggrieve acidic medium.

Different types of adsorption may be considered for the adsorption of inhibitors at the metal surface.

i- Electrostatic attraction between charged molecules and charged metal.

ii- Interaction of unshared electron pairs in the molecule with metal.

iii- Interaction of π-electrons with the metal.

iv- Combination of the above [34].

3.4.1 Inhibition by natural occurring substances.

Natural products act as an easy and cheap way to forbidden or retarding the electrochemical corrosion reaction. It can be gained and extracted by simple aqueous media from many wastes of agriculture plants and seeds without any over much cost with the comparison of synthetic organic materials. The use of these products in many times does not cause any pollution and toxic to the environment. In addition, the fact available on the application of natural products as restrainer in pickling, descalling or polishing processes [138]. Moreover, the advantage of natural products, it can be easily obtained from cheep plants and/or by products (peels, seeds, etc.) remaining in the caning industry, but also, these extracts always contain more than one organic products, these contents of natural product are made it as effective inhibitors in retarding the dissolution of metals.

i) Lawsonia extract.

The obtained results indicated that lawsonia extract perform good inhibition for tin electrode in $NaHCO_3$ and NaCl solutions. Also, inhibit the pitting corrosion of tin. The main components of lawsonia extract are hydroxyl aromatic compounds such as tannin, also present in licorice root and carob, and lawsone. The inhibitive action of tannin was attributed to formation of a passivating layer of tannate on metal surface [139-140]. Tannin is also known to form complex compounds with different metal

cations, especially in the basic medium. For these reasons it is used in the manufacture of anti-rusting paints and coating. Therefore, formation of tannis complexes may be responsible for the observed inhibition in the alkaline medium.

The other constituent of the extract is lawsone which is present in higher amount. Lawsone molecule is a ligand that can chelate with tin to form complex compounds. The formation of insoluble compounds by combination of the Sn^{2+} and lawsone molecules adsorbed on the metal surface is a probable interpretation of the observed inhibition action of lawsone.

ii) Licorice root extract.

The extract of licorice root used to inhibit the general corrosion of tin in $NaHCO_3$ and NaCl solutions and pitting corrosion of tin in $NaHCO_3$ as mentioned above in chapter three. The chemical structure of this extract contains poly aromatic compounds contained glycyrrhizin. These compounds present in licorice root are horizontally adsorbed on the tin surface due to the presence of more than one active centre in the compounds. The adsorption process follow Freundlich adsorption isotherm as maintained above. The strong adsorption process leads to increase the inhibition efficiency and marked shift of pitting potential to more positive (noble) direction.

iii) Carob extract.

The extract of carob was used in this study. The obtained results showed that the extracted of carob acts as an inhibitor for general and pitting corrosion of tin in $NaHCO_3$ and NaCl solutions as mentioned above in chapter three.

As mentioned in the experimental part in chapter two, the carob extract contains mainly sucrose compound. The inhibition of this extract can be explained in view of adsorption of sucrose compound on the tin surface making a barrier for mass and charge transfers. This arrangement leads to protection of the metal surface from the attack of the aggressive anions. The degree of protection increases with increasing of the surface fraction occupied by the adsorbed molecules. As the extract concentration is increased, the number of the adsorbed molecules on the surface increases.

3.4.2 Inhibition by inorganic compounds.

In order to give more information about the role played by some inorganic compounds e.g. the sodium salts of CrO_4^{2-}, MoO_4^{2-}, WO_4^{2-} and HPO_4^{2-} ions toward the general and pitting corrosion of tin was studied.

The inhibitive effect of these anions may be associated with their low polarizability. These anions are expected to concentrate in the diffuse part of the double layer and inhibit corrosion through the reduction of the zeta potential at the oxide film/solution interface. This reduces in turn the potential field and retards the electrochemisorption of the Cl^- ions from the solution on the oxide film.

The polarizability of an anion can be measured to be directly related to its adsorability [141], it can be concluded that inhibition process is due to their adsorption on the electrode surface. The anions that are strongly adsorbed on the electrode surface act as effective inhibitors.

Such inhibition effect of the cited inorganic anions could be better explained by the involvement of these anions in the redox reactions occurring at the electrode surface. The ability of the inhibitor to oxidize

the surface, either the metal atoms or the corrosion product, and its oxidation power play the main roles in this process. The redox reaction is always produced by an adsorption step in which the inhibitor ions adsorbed on the active sites [142], and then, oxidation of these sites take place. The reduced form of the inhibitor may be incorporated in the formed passive film or may go in solution if they form soluble complexes. The oxidation process, therefore, leads to the repair of any flawed regions on the surface and a stable, compact and homogenous barrier film is formed.

The shift of the pitting potential in the positive (noble) direction upon adding increased concentrations of the inhibitive anions could be explained in term of the oxide film theory of passivity proposed by Hoar. et. al [143] as due to the penetration of the inhibitive anions through the oxide film on the metal surface, contaminating the oxide film making it a better ionic conductor, thereby, favoring oxide growth and pitting inhibition. On the other hand, Lecki and Uhlig [144] attribute this behavior to the competitive adsorption of the inhibitive anions with the Cl^- ions on the surface of tin, thus preventing the Cl^- ions from the sites through which it preferentially adsorbed on the passive film and, therefore, decrease the tendency for pitting corrosion. This requires a potential shift to more noble values so as to enable the Cl^- ions to reach concentration in the double layer sufficient to displace the passive film forming species, thereby destroying passivity and initiating pitting corrosion.

The order of inhibition efficiency decreases in the following order in case of $NaHCO_3$ solution:

$$CrO_4^{2-} > WO_4^{2-} > MoO_4^{2-} > HPO_4^{2-}$$

but in case of NaCl solution:

$$CrO_4^{2-} > HPO_4^{2-} > WO_4^{2-}$$

From the above sequence of inhibition efficiency, it is clear that CrO_4^{2-} ions have the best inhibitive action. Several mechanisms have been forwarded to explain the role of CrO_4^{2-} ions in corrosion inhibition. Mc Cafferty [145] showed that, inhibition by chromate can be explained on the basis of a competitive adsorption between the inhibitive chromate ions and aggressive Cl^- ions. If chromate adsorption predominates on the open surface, the passive film formed must involves Cr_2O_3 or $Cr(OH)_3$ [146] . However, if adsorption of Cl^- ions predominates a pitting corrosion will occurs for the free surface.

XPS [147] studies of the passive anodic films showed that, Cr^{6+} ions are reduced to Cr^{3+} ions with the formation of protective Cr_2O_3 and some CrO_4^{2-} ions remain unreacted and incorporated in the film formed on the metal surface.

The molybdate anions play direct role in the inhibition process through the formation of a protective passivating layer of molybdenum oxide of law valency. The passivation occurs also as result of specific adsorption rather than due to inhibitor concentration.

Pryor and Cohen [148] found that, the inhibition efficiency of molybdate is less than that of CrO_4^{2-} ions. This behavior is almost due to strong oxidizing ability of chromate, which leads to the rapid formation of the passive film on the metal surface in the absence of dissolved oxygen. Molybdate being a much weaker oxidizing agent than chromate could not be a strong passivator in the absence of oxygen. It was suggested that in aerated environments oxygen is considered as the primary passivator, and the inhibiting anion action is only film repairing.

The positive shift of the pitting potential of tin electrode with increasing concentration of molybdate anions indicates an increased protective ability of the film formed on the metal surface. This increased protective nature of the passive film may be a result of film strengthening through increased incorporation of adsorbed molybdate into the tin oxide films or due to the increased availability of the adsorbed molybdate ion to repair the defects in the passive film. The dependence of the tin passivation on molybdate adsorption suggests as with many other inhibitors that aggressive anions could be compete the inhibitor adsorption sites on the surface and determinately influence passivation.

The inhibitive action of tungestate ions is found to depend on the aggressive Cl^- ions concentration. The tungestate ions are strongly adsorbed on the metal surface which posses a protective film on the tin surface.

The phosphate anions can not be reduced electrochemically, the inhibitive effect of these anions can be attributed to:

I) Their competitive adsorption on the metal surface.

II) The formation of an adsorbed layer on the oxide film.

III) Formation of a highly insoluble salt with dissolved metal ions which prevent the penetration of aggressive Cl^- ions and consequently decreases the rate of pitting corrosion.